STRUCTURAL ANALYSIS OF HUMAN AND BOVINE BONE FOR DEVELOPMENT OF SYNTHETIC MATERIALS

A Thesis

by

EUNHWA JANG

Submitted to the Office of Graduate Studies of
Texas A&M University
in partial fulfillment of the requirements for the degree of

MASTER OF SCIENCE

August 2011

Major Subject: Mechanical Engineering

STRUCTURAL ANALYSIS OF HUMAN AND BOVINE BONE FOR DEVELOPMENT OF SYNTHETIC MATERIALS

A Thesis

by

EUNHWA JANG

Submitted to the Office of Graduate Studies of
Texas A&M University
in partial fulfillment of the requirements for the degree of

MASTER OF SCIENCE

Approved by:

Chair of Committee,	Hong Liang
Committee Members,	Harry Hogan
	Susan A. Bloomfield
Head of Department,	Dennis O'Neal

August 2011

Major Subject: Mechanical Engineering

ABSTRACT

Structural Analysis of Human and Bovine Bone for Development of Synthetic Materials.

(August 2011)

Eunhwa Jang, B.E., Korea Military Academy

Chair of Advisory Committee: Dr. Hong Liang

With increasing demands in bone repair and replacement, this research investigates the microstructure, properties and performance of bovine bone, human bone, and synthetic materials. Doing so, experimental approaches were used to examine and compare bones, as well as mimicking nature by developing a synthetic material to repair bones. Experimentally, bovine bone, tumor-free human bone, and cancerous human bone were studied via the small scale mechanical loading test. Failure analysis was conducted via optical and electronic microscopic techniques. Characterization results were used to develop a synthetic material that possesses strength and strain needed as a bone material. Characterizing techniques include a small punch test, scanning electron microscope (SEM), optical microscope and x-ray diffraction (XRD) were used for experimental approach.

The results showed that small punch tests in longitudinal and tangential directions showed different mechanical properties and failure mechanisms. Cancer cells in human bone caused the bone softening and lowered the density. Synthesized epoxy-silicone-geopolymer material had higher deformability than bone. Understanding obtained in this research helps us to develop better synthetic bone materials in future.

This thesis is composed of six chapters. The first chapter covers as an introduction to understand the purpose and motivation of present studies, and this section followed by the details of the motivation and objectives of this research. The third chapter explains experimental approaches that were conducted to meet the objectives. The fourth chapter describes the results and the major discovery of the experiments, and the results will be discussed in the Chapter IV. Finally, the last chapter provides the conclusions and recommendations for future work.

ACKNOWLEDGEMENTS

First, I'd love to give my profound gratitude to Dr. Liang who supported, guided and encouraged my research throughout the course of this work. I'm also very thankful to my committee members, Dr. Hogan and Dr. Bloomfield, for their guidance and support. I also appreciate the Turkey biomedical laboratory, which provided cancerous human bone for my research. They offered the cancerous human bone, x-ray photos, MRI and CT images as well. In addition, they kindly answered my request for bone information.

My group members have given big help in studying material science. Matthew taught me how to do the small punch test (SPT) and gave lots of information about the SPT. Michael and Mike helped me take SEM images, Dr. Subrata Kundu helped get XRD data, and Yan provided biological information. Aracely, Brady, David, Fang, Huisung, Jason, Oliver, Rodrigo and other group members gave kind answers and comments. Mariana gave a lot of information and suggestions for my research. She is more than coworker. Brian was coworker to carry on the first part of this thesis and always stimulate to do good research.

Most of all, I really thank to my husband, mother and family. Without their love and encouragement, I could not finish my study.

I am grateful to my agency, the Republic of Korea Army Headquarters, for this opportunity.

TABLE OF CONTENTS

Page

Page

LIST OF FIGURES

Page

Page

Page

LIST OF TABLES

Page

CHAPTER I

INTRODUCTION

This chapter serves as an introduction to the basics behind the thesis research. It presents bone damages caused by disease and accident and mechanical evaluations of bone. Methods include tested via mechanical testing and ultrasound. Finally, this chapter discusses biomaterials for bone replacement, which includes an introduction to biomaterials, their classifications and importance.

1.1. Bone damage

For several decades, the use of automatized machines, vehicles and people who enjoy sports are increasing due to increasing population and change in life styles. In addition, a number of people doing military activities is increasing [1]. Several reasons for bone damage exist, including age, repetitive wear, accidents, excessive exercise and diseases. Some bone damage heals, but some damage is too severe to heal without bone fixation or replacement. Severely damaged bone needs external cures such as bone graft, bone cement and joints replacement. This section will discuss reasons for unrecoverable bone damage.

1.1.1. Accidents

Human bone is commonly damaged by car accidents, athletic accidents and activities in the military field. As economy, industry and culture develop, more people are able to enjoy free time. Thus, the number of people who enjoy dangerous hobbies such as extreme sports, car racing and hunting is increasing. These dangerous hobbies have a high probability

of bone fracture accidents. Moreover, in childhood young people can succumb to more bone fracture accidents than adults because of immaturity or curiosity. When falling from a high place to the ground, bones hitting the ground absorb shock, force and impact. Often, the bones deform when they absorb the forces and, when the application of the force is complete, the bones return to the original shape. However, when the forces are greater than the bones' capacity to absorb, the bones fracture [2]. In addition, 33% of people who are older than 65 years fall yearly, and around 10~15% of people who fall suffer a bone fractures [3]. In the military field, soldiers obtain various training, such as parachuting training, marksmanship training, throwing grenades, river-crossing, planting a mine and so forth; thus they have higher probabilities of facing danger. Also, local wars and civil wars exist in the world. These wars cause accidents in which civilians strike mines or are shot.

1.1.2. Impact of metastatic cancer and metabolic bone disease

Human bone can be affected by cancer, osteoporosis, osteopetrosis, osteomalacia and so forth [4]. These diseases cause bone loss and/or loss of the mechanical properties of the bone. Osteoporosis is the most common bone disease, and it offers results in hip and spine fractures. Hip fracture from osteoporosis causes people to require pin or plate fixation on their bones [5]. It was considered a disease by aging, but nowadays, the osteoporosis can be rarely observed in young adults and children because of immoderate losing weight [6]. Bone cancer also lowers the bone density because it grows abnormally. A bone tumor that is malignant is classified as bone cancer. Moreover, bone cancers are classified as osteosarcoma, Ewing's sarcoma and chondrosarcoma. The osteosarcoma forms on the osteons, and chondrosarcoma forms on the cartilage or surface of the bone. In addition, the Ewing's

sarcoma forms in the long bones, and this occurs during childhood and adolescence when the bone grows rapidly [7, 8]. Osteopetrosis is a rare disease characterized by bones that harden and become more brittle. This disease causes extremely high risk of bone fracture [9]. Osteomalacia is a bone softening disease characterized by a lack of bone mineral. This disease also induces the risk of bone fracture [10].

1.1.3. Other damages to bones

Immoderate activities, drugs, aging, and insufficient nutrients can contribute to bone fracture. Excessive loading on bone such as too much jumping and/or running can cause stress-induced fracture. The stress fracture starts on a micro-scale, but if bone undergoes use continuously or carries excessive loads or faces an impact, the bone will be fractured. Approximately half a million long distance runners, considerable numbers of military recruits, dancers have stress fractured bones [11, 12]. Aging causes lower bone density and tissue quality [12]. Smoking, consuming large quantities of alcohol for a long time and frequent corticosteroid use can increase risk of bone fracture [13-15]. Smoking lowers the bone density and raises the probability of fracture [13]. When corticosteroids are used for a long time, osteoporosis and bone fracture are much more likely [15]. Furthermore, the corticosteroid causes necrosis of the bone because blood flow to the bone is compromised [16].

1.2. Mechanical evaluations of bone

Studies of the mechanical properties of bones have been done for more than 180 years. In the middle and late 1900s, a number of papers about the mechanical properties of

bone were published [17]. To evaluate elastic modulus, the two major methods used are the direct mechanical loading tests and the acoustic methods [18]. Details of the mechanical loading tests are described in the subsection (See 1.2.1). According to the scale of samples, mechanical tests on bone tissues and whole bone were performed [18]. Acoustic methods have several advantages, which are non-destructive process, versatility, small specimen size and repeatability of the measurements. The three primary methods are ultrasonic velocity measurement, acoustic microscopy and critical angle analysis [19]. For the ultrasonic velocity measurement, the velocity of sound can be calculated by measuring the conveyed wave. The ultrasonic velocity measurement is a feasible method to study the mechanical properties of trabecular bone [20]. Acoustic microscopy measures the time retardation of reflected wave by the top and bottom surface of the bone by using a focused beam of acoustic energy [19]. Figure 1 shows the acoustic microscopy. For critical angle analysis, the specific angle at which all transmitted energy was reflected and no energy refracted, determines the acoustic velocity [21].

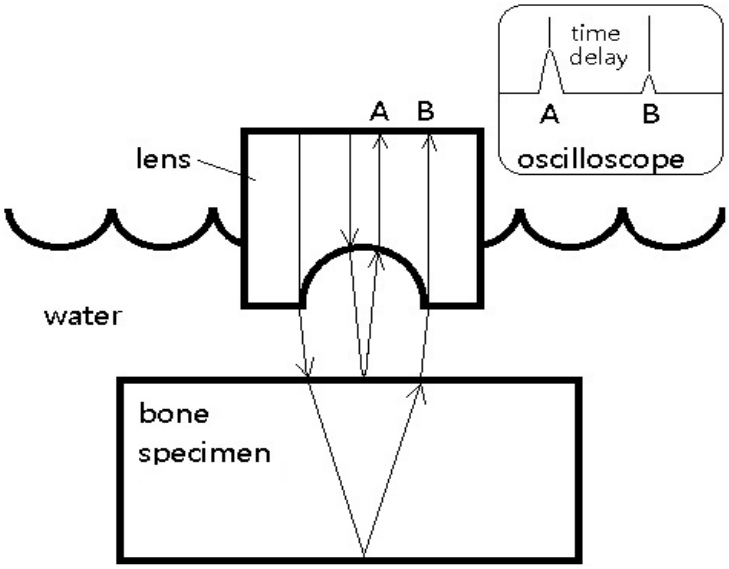

Figure 1. The acoustic microscopy

1.2.1. Mechanical loading tests

Mechanical tests for include tension, compression, bending, torsion, indentation, shear and fatigue tests [19]. The direct mechanical loading tests are appropriate to apply cortical bone and cancellous bone. The tensile test is the most precise mechanical test because it does not involve bending moments [19]. The compression test requires smaller samples. For example, the tensile test uses 15~40mm long [22] and 2~6mm diameter [23] samples, but the compression test uses 7~10mm cubes. However, because of its end effect and possibility of buckling, this test is less precise than the tensile test [19]. Misaligned specimens to the loading plate can undergo stress concentration, and buckled one can face bending moment. This two unexpected phenomena cause underestimated Elastic modulus and strength [19]. Figure 2 shows (a) the end effect of misaligned specimen and (b) the buckled specimen (b) during compression test. The bending test is a feasible method to

measure the mechanical properties of long bones, especially of small animals[19]. This experimental method is suitable to observe fractures induced by bending motions. Indentation tests are appropriate to measure the mechanical properties of cartilage and trabecular bone. These tests are conducted with a 2.5~6mm diameter rounded indenter and 0.2~0.5mm depth into the samples [19].

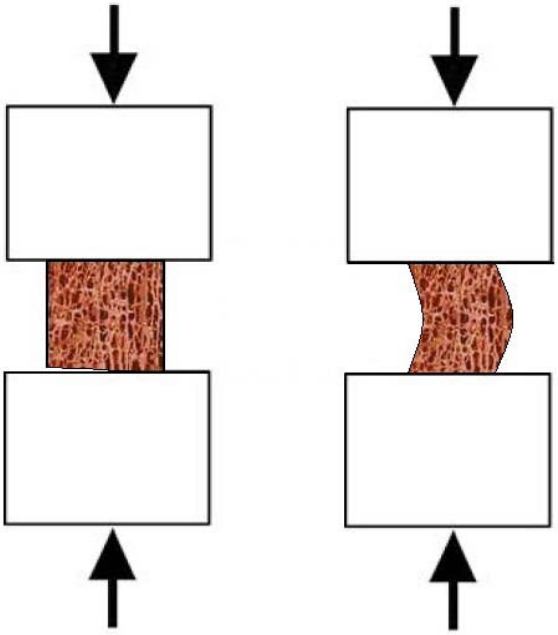

(a) (b)

Figure 2. (a) The end effect of specimen (b) the buckled specimen during compression test

1.2.2. Small scale test

The number of micro-scale and the nano-scale mechanical tests is growing. Generally used materials are individual trabeculae, single osteons and individual lamellae. Many

mechanical loading tests mentioned in the previous section were conducted on this small scale [19]. Ascenzi and his co-researchers used single osteons for the mechanical tests. The sample size was 180~300 μm wide [24, 25] and 300~500 μm long [26, 27]. Effort and care are required to prepare these micro-size samples. Moreover, the Young's moduli of cortical human bone measured via bending test depended on the sample size, because smaller samples have more stress concentration factors [28]. Micro- and nano-hardness tests were conducted to measure micron or sub-micron size of the mechanical properties of bone and the quantity and quality of mineralization of the bone were reflected in the hardness tests [19]. The nano-indentation method has been considered as feasible method to measure the mechanical properties of single lamellae, and this demonstrates that the stiffness of the single lamellae depended on the direction of the fibers [29]. Well-polished surfaces of samples were required to conduct these micro and nano scale hardness tests [30, 31].

1.3. Orthopedic biomaterials

1.3.1. Introduction to biomaterials

Biomaterials are synthetic materials used to make implants in order to replace and repair the function of damaged or diseased tissues or organs, to aid healing, to improve or augment organ operation, and to correct unnatural functions or deformities in contact with living tissues [1, 32, 33]. Since the 1860s, when Lister developed the complete antiseptic surgery technique, the use of synthetic biomaterials has increased immensely [34, 35]. In the 1890s, the first implant, a bone plate made of vanadium steel, was introduced. However, it was unsuccessful because the vanadium steel corroded swiftly in the body. The next biomaterial used was stainless steel and cobalt chromium alloys in the 1930s. After World

War Ⅱ, PMMA was added to the biomaterials [33]. Approximately four to five million implants are used each year [34], and approximately one million bone grafting surgeries are performed each year in the world [36]. Global market for orthopedic technology and products will reach roughly $32.4 billion by 2015 and is expected to grow with an annual average rate of 2.7% from 2009 [37].

1.3.2. Classification of biomaterials

Biomaterials are classified as materials or tissue reactions. Materials include metallics, ceramics, polymerics, and composites [1, 32, 33]. Tissue reactions include bioinerts (Metals, Alumina, Zirconia, PMMA), bioactives (bioactive glass, Hydroxyapatite) and biodegradables (Tricalcium phosphate, Hydroxyapatite, PLA, PGA) [32, 38, 39].

Metallic biomaterials are widely used and have played an important part in replacing or repairing damaged bone [1, 40]. Stainless steel, Titanium and Ti alloys, cobalt chromium alloys and magnesium alloys are used as metallic biomaterials [40, 41]. Metal has high strength, high toughness, high ductility, and resistance to wear [1, 32]. However, the metallic biomaterials have limitations which are high density, mismatch of elastic modulus with bone and liberation of the ions and/or particles in the body [1, 32, 40]. High density metallic biomaterials can cause heavy implants, and this would likely lead to an unbalance between the right and left sides of the body. The metallic biomaterials have 10~20 times higher elastic modulus than bone, and this can cause stress shielding. Stress shielding can cause bone weakening and loosening of implants by reducing stimulation of bone growth because bone carries less load than the implants [32, 40]. Since metals can liberate the ions and/or particles, allergic reaction and loss of tissues may result [32, 40]. The usual uses of metallic

biomaterials are for stems of artificial joints, heads of artificial joints, and fracture fixations (pin, screw, plate) [1, 40, 41].

The most commonly used ceramic biomaterials are alumina, zirconia, hydroxyapatite, calcium phosphate and bioactive glass. These ceramic materials are well-known for their corrosion resistance, wear resistance, biocompatibility, high compressive strength and creep resistance [32, 33, 39]. Moreover, bioactive ceramic materials chemically bond with bone tissues, and biodegradable ceramic materials were resorbed and cause the surrounding tissues to replace them [42]. However, ceramic materials are brittle and have low tensile strength, low impact strength, and low fracture toughness. In addition they are difficult to manufacture [1, 43]. Their uses are for bone fracture fixations (plates and screws), heads of artificial joints, coatings on the metallic stem of artificial joints, bone replacement and bone cement [43].

As polymeric biomaterials, polyethylene (PE), polypropylene (PP), polymethyl methacrylate (PMMA) and polylactide (PLA) are used for bone replacement and artificial joints [43]. The polymeric biomaterials are flexible, easy to fabricate, cheap and have low density when compared to metallic and ceramic biomaterials [39, 43]. However, they have low strength, low fracture toughness, more rapid degradation in human body, low thermal resistance and susceptibility to UV [43-45]. Released particles, monomers and oxygen from cross-linking polymers can cause irritating tissue and decreasing strength [1, 32]. The uses are for cups of artificial joints, bone fracture fixation and bone cement [33, 43]. In particular, polypropylene is used for finger joint implants because of its remarkable flexibility [34, 43]. Table 1 shows the applications of each classification of biomaterials and their references.

Table 1. The applications of biomaterials

Classification	Materials	Applications	References
Metal	316L Stainless steel	Bone fracture fixation Artificial joints	[1, 32, 41, 46]
	Titanium and Ti alloys	Bone fracture fixation Artificial joints	[1, 32, 41, 46]
	Cobalt chromium alloys	Bone fracture fixation Artificial joints	[1, 32, 46, 47]
	Magnesium alloys	Bone fracture fixation	[40]
	Nickel titanium (shape memory alloy)	Bone fracture fixation Spinal implant	[46]
Ceramic	Alumina	Artificial joints	[1, 43]
	Zirconia	Artificial joints	[1, 43]
	Hydroxyl apatite	Bone defect repair Implant coating Artificial bone graft	[1, 48, 49]
	Calcium phosphate	Bone defect repair Implant coating Bone filler	[1, 38, 48]
	Bioactive glass	Implant coating Bone filler	[1, 5]
Polymer	Polyethylene	Cups of artificial joints	[32, 33]
	Polypropylene, PET	Finger joints implant	[32, 34, 43]
	PMMA	Bone cement Bone filler	[33, 43, 50]
	PLA, PGA	Bone deficiency repair Bone fracture fixation	[38, 51]

1.3.2.1. Composite biomaterials

Composite materials are created by combining two or more different materials to improve mechanical properties of the materials [34]. The most commonly used composite biomaterials include polyethylene/hydroxyl apatite, silicone/silica, epoxy/carbon fiber, alumina/hydroxyl apatite and PEEK/carbon fiber [5, 32]. The composite materials have high strength, proper elastic modulus, and some have bioactive and biodegradable properties [32, 34]. Moreover, desirable properties can be achieved by changing the volume fractions of reinforcement and the structure [32, 43]. However, composite materials are difficult to mold. In addition, the polymeric matrix of composite materials releases debris and absorbs water [1, 43]. When the polymer matrix absorbs water within the body, the strength and stiffness of composites decreases [43]. The uses of bio-composites are bone fracture fixation, artificial joints and bone cement [1, 34, 43]. Although composite materials have a smaller elastic modulus than metals and ceramics, the value is still higher than bone. Also, the loss modulus of composite materials is much lower than bone [52, 53]. Recently, degradable glass fiber reinforced polymer composite materials have been considered for biological applications because the materials degrade in the human body; however, the fibers and matrix of the degradable composite material separate in vivo. Therefore, the material's mechanical properties suffer as a result. [54]. The composite material's elastic modulus must either be equal to or slightly less than bone. The reinforcement and the matrix must not separate in vivo in order to function properly.

CHAPTER II

MOTIVATION AND OBJECTIVES

As discussed in the first chapter, the need for replacement bone and/or bone fracture devices has been increasing because the numbers of people, who enjoy extreme sports, participate in military activities and use automatically operated machines and vehicles are increasing. Also, bone has unique properties so that it is not easy to develop perfectly replaceable material. Thus, a large quantity of effort has been dedicated to this area.

The aims of this research are understanding failure mechanisms of bones and development the new synthetic material. To develop proper synthetic materials, investigation of the physical, mechanical properties of the origin material must precede. The mechanical properties of the biological material can be determined by the small punch test, and the mechanically and structurally mimicked materials can be formed.

This research was conducted to get two objectives:

1. Acquire understanding of the material behavior of the different directional bovine bones and tumor-free and cancerous human bones by the small punch test and microscopic images.
2. Synthesize new material for artificial bone and bone fracture devices motivated by the bone structure.

These objectives are important to understand the fracturing behavior of the structure of the bone and the application of new materials for bone replacing and cure. From the achievement of this research, the structure of biomaterials for artificial bone can be improved.

The following chapters contain experimental methods and analysis. First, decontamination process will precede bone sampling. To evaluate the mechanical properties and to obtain failure of the bone samples, small punch test will conduct. Via optical microscope and scanning electron microscope, failure mechanism will analyze by observing the fractured surfaces. Based on this structure analysis, the synthetic material will be formed.

CHAPTER III

EXPERIMENTAL PROCEDURE

This chapter describes materials to be studied, the preparation procedure, and characterization methods. Human bone samples obtained from collaborators were used for this study. Techniques used to prepare them for small punch tests are discussed in this chapter. Various characterization techniques used to study properties of bone samples are introduced. This chapter contains three sections, materials, sample preparation, and their properties along with methods to obtain them. Finally, materials mimicking human bones were developed. Synthesis procedures are discussed here.

3.1. Materials

3.1.1. Bovine bone samples

The cow shank pack was purchased from a local commercial supplier. Typically, 30 month-old steers and heifers were used for daily consumption [55]. The shank part was femur of bovine and compact bone part of femur was used for the test. Figure 3 shows the locations of bovine femur and humerus.

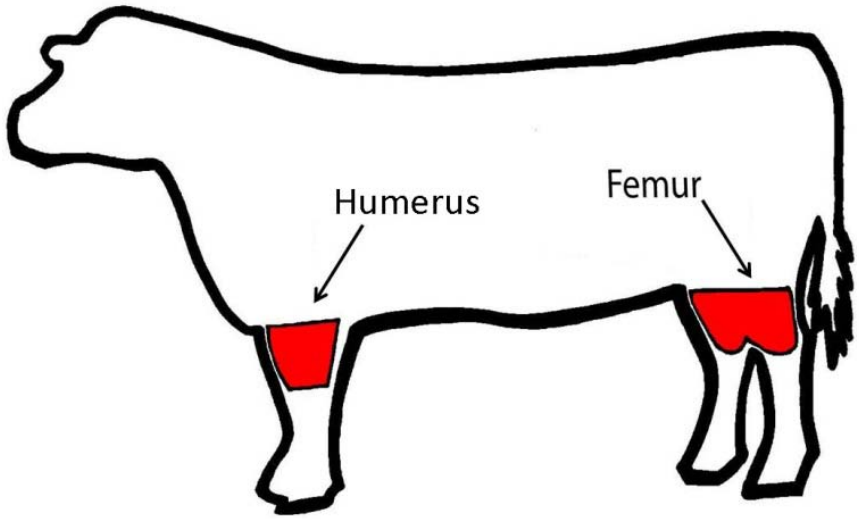

Figure 3. The location of bovine humerus and femur

3.1.2. Human bone samples

Two kinds of human bones were used for this study. One was a tumor-free human bone, and the other was a cancerous bone. The tumor-free human bone was from a patient who was 51years old male and amputated because of ischemic necrosis from vascular obstructive disease[56]. The bone was stored in freezer which was preserved at the temperature of -17℃. The part of the bone was tibia and the center of tibia compact bone was tested. The cancerous bone was obtained by collaborating lab in Turkey (Bogazici University, Institute of Biomedical Engineering) [56]. It was sterilized with 70% denatured ethanol for 60 minutes according to the standard procedure of Depaula et al. [57] and wrapped around by paraffin. The bone was tibia, and proximal part of the cancellous and cortical bone was infected by cancer cell. Regarding the age bone, this is expected to have lower strength and

mineral density than tumor-free bone of 12-year-old human [58-60]. Table 2 shows the information of the bones.

Table 2. Background information of tested bones

Information	Bovine	Human	
		Tumor-free	cancerous
Originality	Commercial supplier	Collaborating lab	Collaborating lab
Age	30 month	51 years	12 years
Gender	Unknown	Male	Female
Part	Humerus, Femur	Tibia	Tibia
Comments	None	Vascular obstructive disease	Contracted cancer (Ewing sarcoma)

3.1.3. Synthetic materials

Epoxy, silicone and geopolymer powder were used to make new composite material. These two materials were chosen based on their loss modulus and compression strength. Figure 4 is the bubble chart of biomaterials, and it shows the compressive strength and loss modulus of each material. Blue lozenges and bubble represents those two mechanical properties of bone, green triangles and bubble represents that of silicone, and green circles and bubble represents that of polyepoxide. As shown in the figure 4, silicone has a high loss modulus, and polyepoxide has high compression strength. New material made of these two

materials is expected to have those two high values. The epoxy was composed of 150 thick epoxy resin and epoxy hardener manufactured by US Composite (West Palm Beach, Florida). The silicone was manufactured by General Electric Company (Huntersvile, North Carolina, USA) and purchased at local commercial supplier. The geopolymer was made of Metakaolin (MetaMax®, BASF catalysts LLC, NJ), which has 53%wt SiO_2 , 43.8%wt Al_2O_3 and 3.2%wt of other impurities, and sodium silicate solution by the High Temperature Materials Lab in the Texas A&M University. It was ground with a pestle and a mortar by hand and for two hours. To create the layered structure, epoxy and silicone was applied alternately with an art brush on the glass plate. Firstly, the silicone was spread thin on the glass plate with brush and the geopolymer powder was sprinkled on the wet silicone layer. The silicone layer held the geopolymer powder well. Then the epoxy was spread on the geopolymer sprinkled silicone with brush. The thickness of each layer was approximately 40μm, particle size of geopolymer powder was 10μm, and the each layer was dried at room temperature for 5 hours.

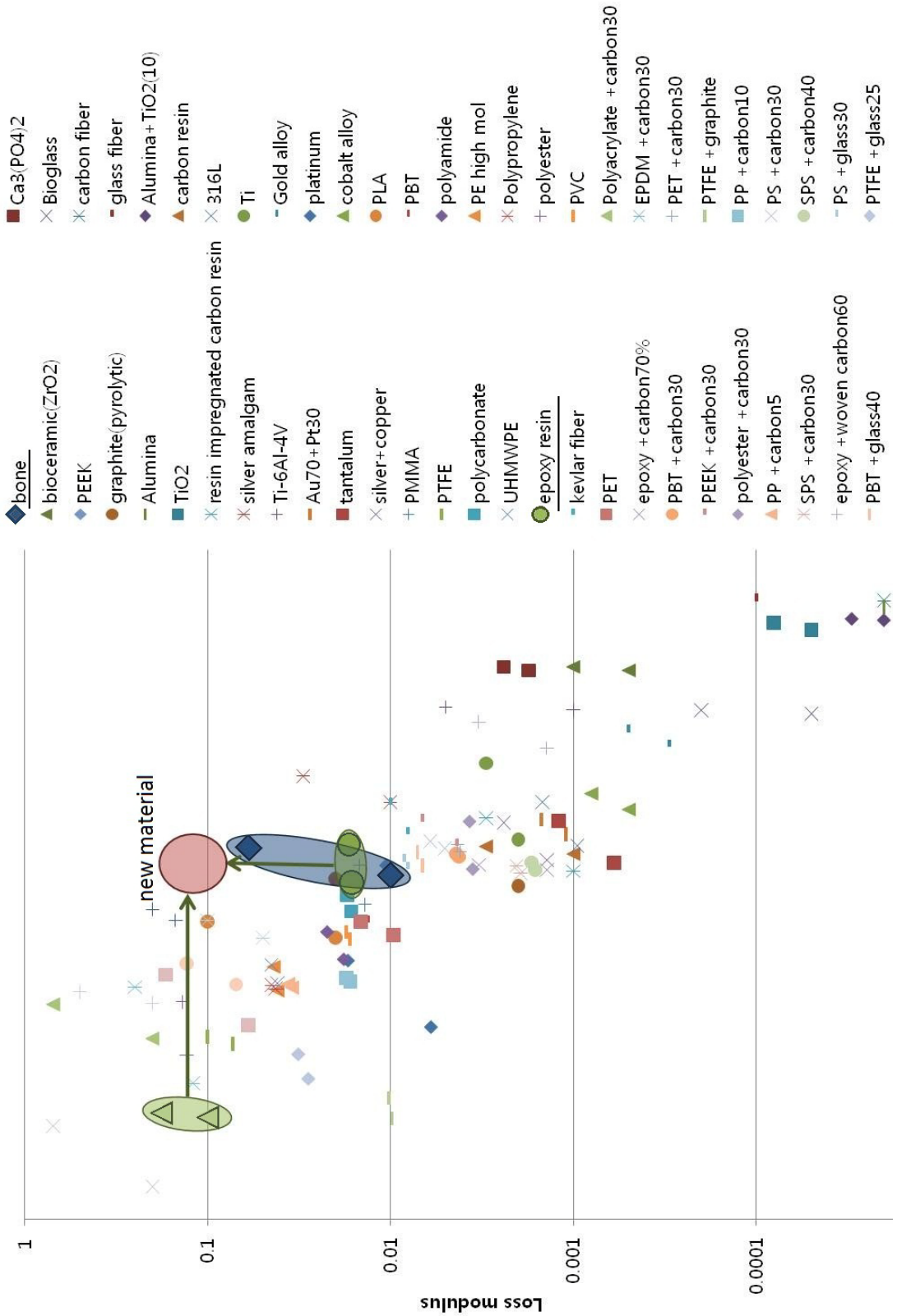

Figure 4. Bubble chart of biomaterials with compression strength and loss modulus

3.2. Specimen preparation

3.2.1. Bovine bone

The marrow in the center of the shank bone was removed as well as soft tissues. Bones were cut into slices of 2~3mm of thickness using a hacksaw and were ground 2mm of thickness with a 120 grit sand paper. The bone sheet was then cut into 35 small sample slices of 2~3cm width by using a Dremel tool. These were left for 24 hours to be dried after being rinsed with flowing water followed by bacterial culture was conducted. Then, the 35 small sample slices were cut into cylinder of 3mm diameter with milling machine in machine shop of the mechanical engineering department. The diamond coated drill bit of which inner diameter was 3mm, was used with milling machine. Figure 5 shows the drill bit and figure 6 shows the final shape of bone sample for the small punch test. Overall, 96 cylindrical samples were gotten. These samples will be used for the small punch test.

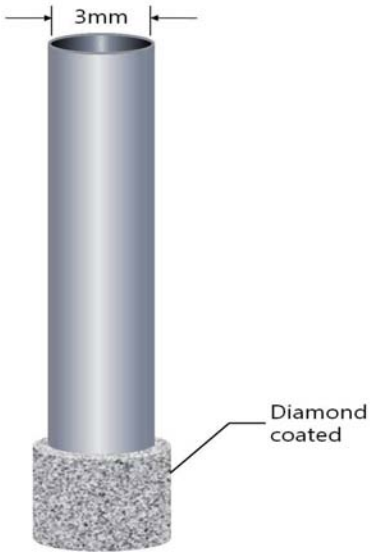

Figure 5. Diamond coated drill bit

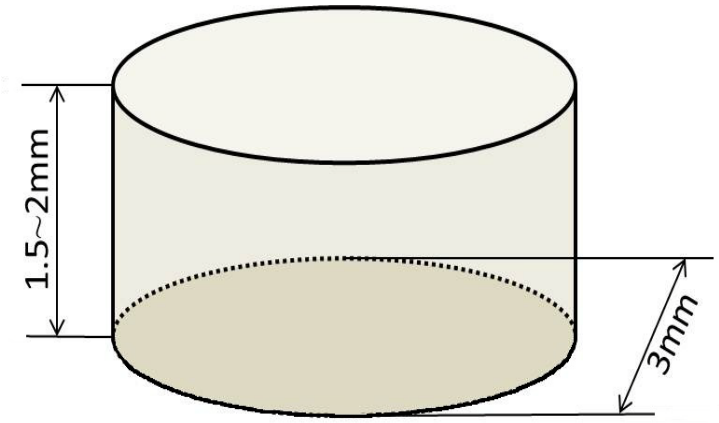

Figure 6. Cylindrical bone sample shape for small punch test

For small punch test on three different directions, the bovine bone had to be cut in corresponding methods. The center empty cylindrical bovine bone lumps were cut in three different directions. Figure 7 illustrates the sample direction in correlation with the main axis direction. For testing on longitudinal direction, the 1 inch long bovine shank bone was cut in the direction parallel to x-y plane. Another bone mass was cut in the direction parallel to x-z plane and y-z plane to radial test, and the other bone mass was cut along the radial direction for test in the circumferential direction. The bone masses were cut in thickness of 3mm and the bone slices were polished until that the thickness became 2mm. Then the bone slices of 2mm thickness were attached on wood piece and milled with milling machine and the drill bit to be cylindrical samples of 3mm diameter.

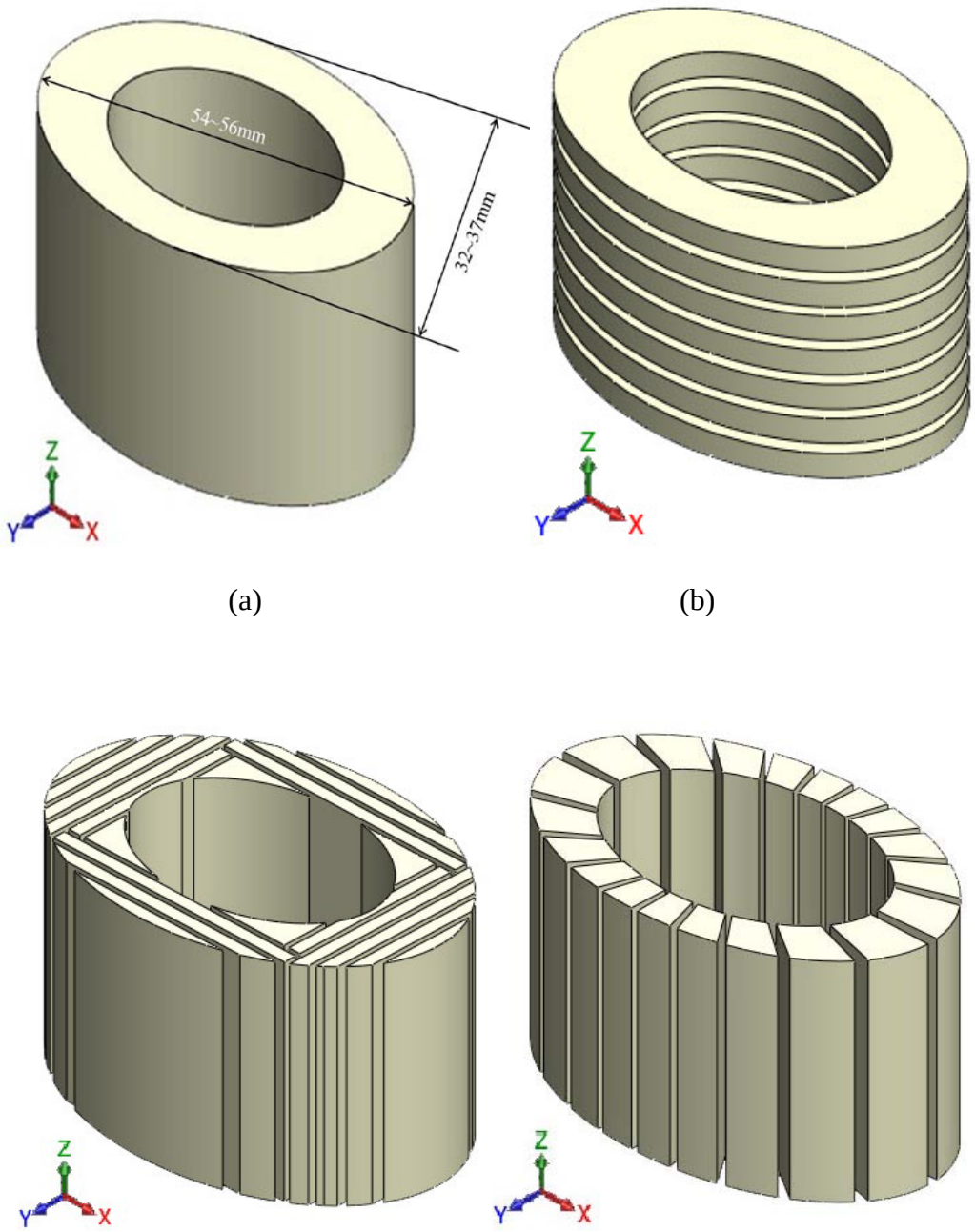

(a) (b)

(c) (d)

Figure 7. (a)Whole bone (b) cutting to test longitudinal direction

(c) cutting test radial direction (d) cutting to test circumferential direction

3.2.2. Human bone

For preparations of sample with human bone without tumor cell, the center of tibia was used. The one inch long bone mass of human tibia was too small to be held by a vise. More precise equipment was needed. Therefore, slice of the bone was cut with the IsoMet® 1000 Precision saw (Buehler, Lake Bluff, Illinois, USA) and attached on the wood block. The cutting direction was perpendicular to the axial direction. Figure 8 shows the precision saw, and figure 9 shows the slices of tumor-free human bone. The attached bone had remained 24 hours at the temperature of 4℃ for sure to be attached on the wood. Then a milling machine in the machine shop of the mechanical engineering department was used to make 3mm diameter cylindrical samples. The cancerous bone was cut with hacksaw in thickness of 3mm because it was relatively weak than tumor-free human bone. The slices were cut with thin blade to make 3mm diameter of cylindrical samples.

Figure 8. IsoMet® 1000 precision saw

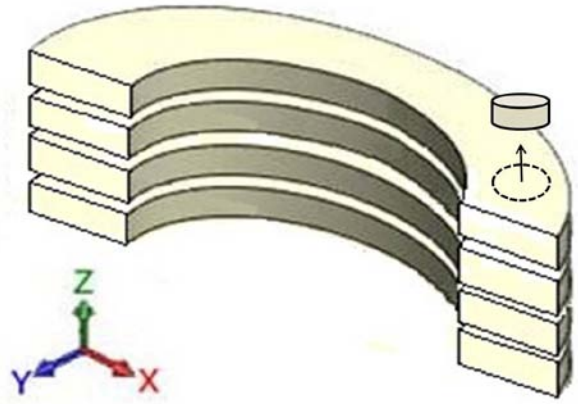

Figure 9. Slices of tumor-free human tibia

3.2.3. Synthetic materials

The dried synthetic materials were cut as 3mm diameter of cylindrical samples with milling machine in the machine shop of the mechanical engineering department. The homogeneous samples were ground with sandpaper to make 2mm of thickness. The layered samples were adjusted the thickness to be 2mm when they created. Eight cylindrical synthetic material samples were attached on the bovine bone machined perpendicular to the axial direction. Six cylindrical synthetic material samples were attached on the bovine bone samples machined for radial test. The adhesive was epoxy resin which was the same material to be used for making the synthetic material.

3.2.4. Chemical treatment

Two cleansing solutions were used: isopropyl alcohol ($(CH_3)_2CHOH$) and hydrogen peroxide (H_2O_2). The reasons to treat bovine bone were to avoid infection and to study the effect of the chemical solutions on the bovine bone. Sixteen conditions of each solution were used to treat the bovine bone samples. The sixteen conditions of hydrogen peroxide were 3%wt, 5%wt, 10%wt, and 20%wt concentrations and each concentration treated sample for 10, 30, 45, and 60 minutes respectively. The sixteen conditions of isopropyl alcohol were 10% wt, 30% wt, 50% wt, and 70% wt concentration and each concentration treated sample for 3, 5, 10, and 20 minutes, respectively. The samples in the control group were treated with distilled water for ten minutes. Table 3 shows the sixteen conditions of chemical solutions and control group treatment.

Table 3. Treatment conditions of chemical solution and control group

Group	Concentration	Soaking time
Control	-	10 min.
Hydrogen peroxide	3% wt	10 min.
	5% wt	30 min.
	10% wt	45 min.
	20% wt	60 min.
Isopropyl alcohol	10% wt	3 min.
	30% wt	5 min.
	50% wt	10 min.
	70% wt	20 min.

3.2.5. Bacteria culture

First of all, 23g agar powder and 1ℓ distilled water were uniformly mixed by hands to make agar followed by being sterilized using an autoclave machine model 57CR (American sterilizer company, Erie, Pennsylvania, USA) for 25 minutes. The hot agar colloidal fluid was poured into the 10cm diameter of petri dishes and left for 24 hours to be cooled and hardened. Without any instant contamination, the 35 small bovine cortical bone sample slices were swiped with cotton swabs and the cooled agar plates were swiped with the cotton swabs. This process was performed on the disinfected desk with 70% wt of ethanol. The swiped agar plates were incubated in the incubator for 120 hours [61]. While incubating, the 35 small bone sample slices were treated with sixteen conditions of hydrogen peroxide and isopropyl alcohol. The treated samples were surrounded by 40℃ air in the oven for 24 hours to be dried. On the dried bone surfaces, the same procedure was used, swabbing using cotton swabs. Other cooled agar plates were swiped with the cotton swabs and incubated for 120

hours in the same incubator. After forming bacteria colonies, the optical microscope was used to count the colonies. All of countable one was counted by 20x~200x magnifications.

3.3. Characterization

3.3.1. X-ray diffraction

X-ray diffraction (XRD) was done to study the microstructure with Bruker-AXS D8 Vario X-ray Powder Diffractometer (Bruker, Billerica, Massachusetts, USA). Bovine bones before and after chemical solution treating were analyzed. One condition of each solution was selected which is the highest concentration and longest soaking time. These strongest chemical solutions have more possibility to alter the crystalline property of the bovine bone. When the x-ray beam impinges upon the material, a part of the beam is diffracted in random directions, and two opposite scattering events happen. One is destructive interference, and the other constructive. In most cases, the amplitude of diffracted beam ranged between zero and twice the wave length of the incident beam. The angles between incident beam and the crystal plane equals the angle between the diffracted beam and the crystal plane. Thus, the detector is positioned at twice the angle between the sample and the incident beam. From this method diffracted angle versus intensity plot will be obtained. The width of the peak represents the crystallinity of materials. The XRD was run with 0.04 stepsize, 38 seconds of steptime, and the wavelength was 1.54nm.

3.3.2. Density measurement

The densities of tumor-free human bone and cancerous human bone were measured. The unfractured tested human bones were exposed to flowing air for 48 hours to dehydrate.

The volume of these samples was measured by the program named Image J. The 20x magnification of optical microscopic images of human bone samples were taken, and the thickness and the base area were measured by Image J. The Pioneer Balance scale was employed to measure the weight of the tumor-free and cancerous human tibia samples. (Ohaus Co., Parsippany, New Jersey, USA)

3.3.3. Small punch test

Small punch test was carried out for investigation. The setup is shown in figure 10, and the cross section is shown in figure 11. As shown, it contains an upper jig, lower jig, push rod, and ball. The load on the ball bearing was applied by Instron machine model number 4411 shown in figure 12 and interfaced with a computer showed displacement and load. The velocity of cross head was set at 0.002mm/sec for 6~15minutes. The instron machine was stopped when the upper jig contacted with bone samples. This moment can be noticed by the labview in the computer. The behavior of bone during the small punch test was observed by the labview in the computer, thus the fractured surface under different load was obtained. The test was repeated 1~5 times for chemical effect on separate samples, 5~9 times for different directions, and 6~9 time for human bone specimens. The small punch test was introduce in 1981 by Manahan [62]. This test allowed small volume of specimens, thus more tests could conduct [63]. The ball bearing penetrated the samples to 1mm of depth and more because the diameter of the ball bearing is 1mm [64], thus mechanical evaluation of surfaces as well as inside of samples. Besides, various specimen behaviors can be observed during the small punch test, such as, indentation, buckling, and fracture.

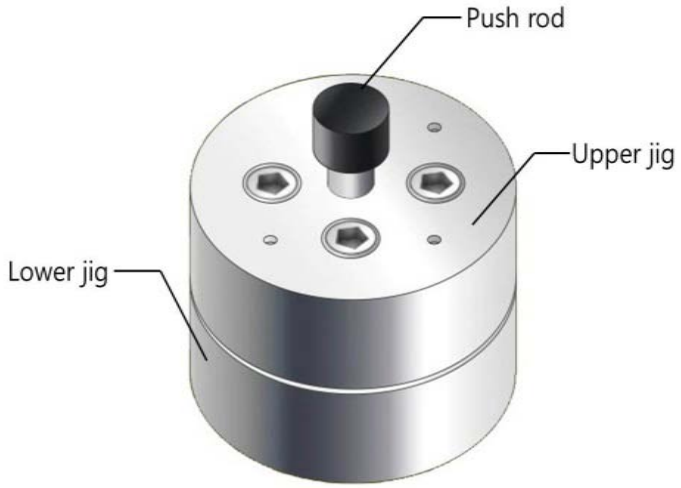

Figure 10. Overview of the small punch test jig

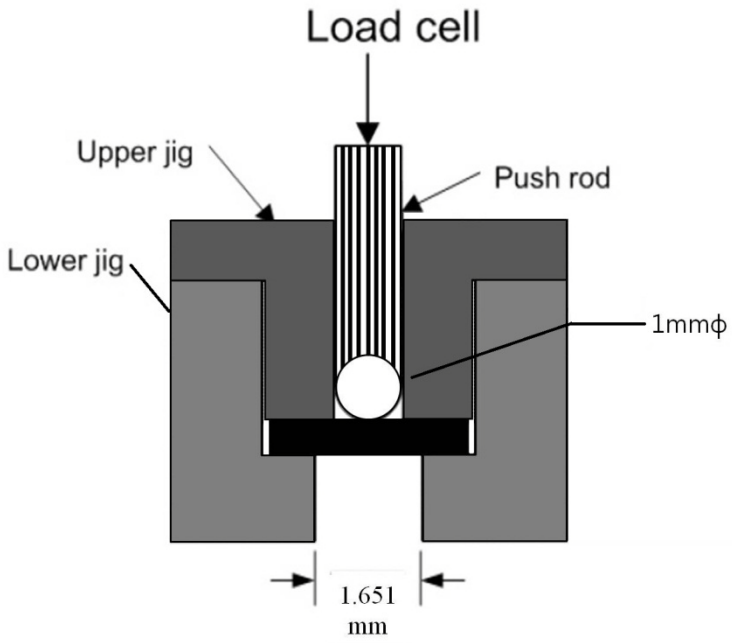

Figure 11. Cross-sectional view of the small punch test jig

Figure 12. Instron machine model 4411

$$F = \frac{4}{3} E^* R^{\frac{1}{2}} d^{\frac{1}{2}} \qquad (1.1)$$

$$\frac{1}{E^*} = \frac{1-\nu_1^2}{E_1} + \frac{1-\nu_2^2}{E_2} \qquad (1.2)$$

To obtain elastic modulus of three directional bovine bones, the Hertzian contact theory was used [65]. The bones were assumed to be isotropic. The equations (1.1) and (1.2) were from the Hertzian contact theory. “F” is load, “R” is the radius of ball bearing, “d” is indentation, “v_1” is the Poisson’s ratio of the bone, “E_1” is elastic modulus of bone, “v_2” is the Poisson’s ratio of the steel ball bearing, and “E_2” is elastic modulus of steel ball bearing. The radius of the ball was 0.5mm [64], the elastic modulus of the stainless steel ball bearing was 206GPa, and the Poisson’s ratio of the ball was 0.3 [66]. The Poisson’s ratios of the bovine bone were 0.35 for longitudinal test and 0.41 for tangential test taken from Meunier et al. (1989) [67]. The linearly increasing part was selected from the small punch test plot by using the linear trend line in the excel program. Figure 13 shows the selected linear part of

the small punch test plot. The values of displacement and load at the beginning and end of the selected part were obtained. The differences between the two values were calculated. The calculated load value was inserted in the Hertzian contact equation as F (load), and the calculated displacement value was placed in the Hertzian contact equation as d (indentation).

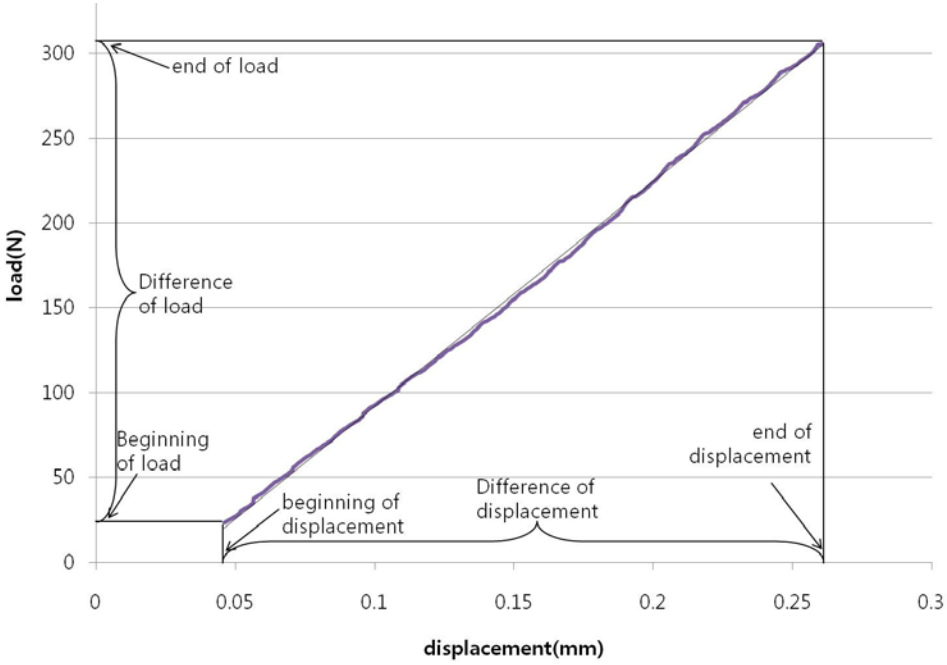

Figure 13. Selected linear part of SPT plot

3.3.4. Microscopic analysis

Microscope images were taken to observe the fractured surfaced obtained after the small punch test. The VHX-600 digital microscope (Keyence, Woodcliff Lake, New jersey, USA) at 100x and 200x magnifications were used for imaging. Transmission mode of light

was used to highlight inner structures due to the translucent structures of bones. Top view which was indented by ball bearing and fractured side view was observed. Figure 14 shows the digital optical microscope.

To more closely observe the surface, scanning electron microscope was used. The Vega Ⅱ LSU (Tescan, Cranberry Township, Pennsylvania, USA) microscope at 70~80x magnifications for overview of the samples and 200x~500x magnifications were used to observe details. For the bovine bone the energy of beam was 10kV, and working distance was 25.504mm. For the human bone samples, 20kV of energy beam and 18.417mm of working distance were applied.

Figure 14. Digital optical microscope

CHAPTER IV

EXPERIMENTAL RESULTS

This chapter describes experimental results of tests which were previously explained. In the first section, the effect of chemical cleansing solutions on the microstructure and mechanical properties of bone materials is explained. In second, the difference of mechanical properties among three different directional bovine compact femur samples by the small punch is illustrated. Lastly, the negative effect of tumor cells on the human tibia via the small punch test is depicted.

4.2.1. Effects of cleansing solutions on the bovine bone

4.1.1. Effects on the microstructure

Figure 15 shows the X-ray diffraction (XRD) results of bovine bones machined for longitudinal test before and after water treatment. The lower blue line shows the untreated sample XRD data, and the upper red line shows the XRD data of the sample treated for 10 minutes in distilled water. The peaks labeled by squares represent the calcium phosphate, and labeled by circles as the hydroxyl apatite. These peaks were distinguished by using the program Jade version 5.0. (Materials Data, Inc., Livermore, California, USA) The two similarly high peaks located at 24.6°, 26° (2θ) in the untreated plot changed to one high peak and one low. Moreover, the highest peak in the plot of the untreated sample at approximately 32.3° (2θ) became narrower after treating with water.

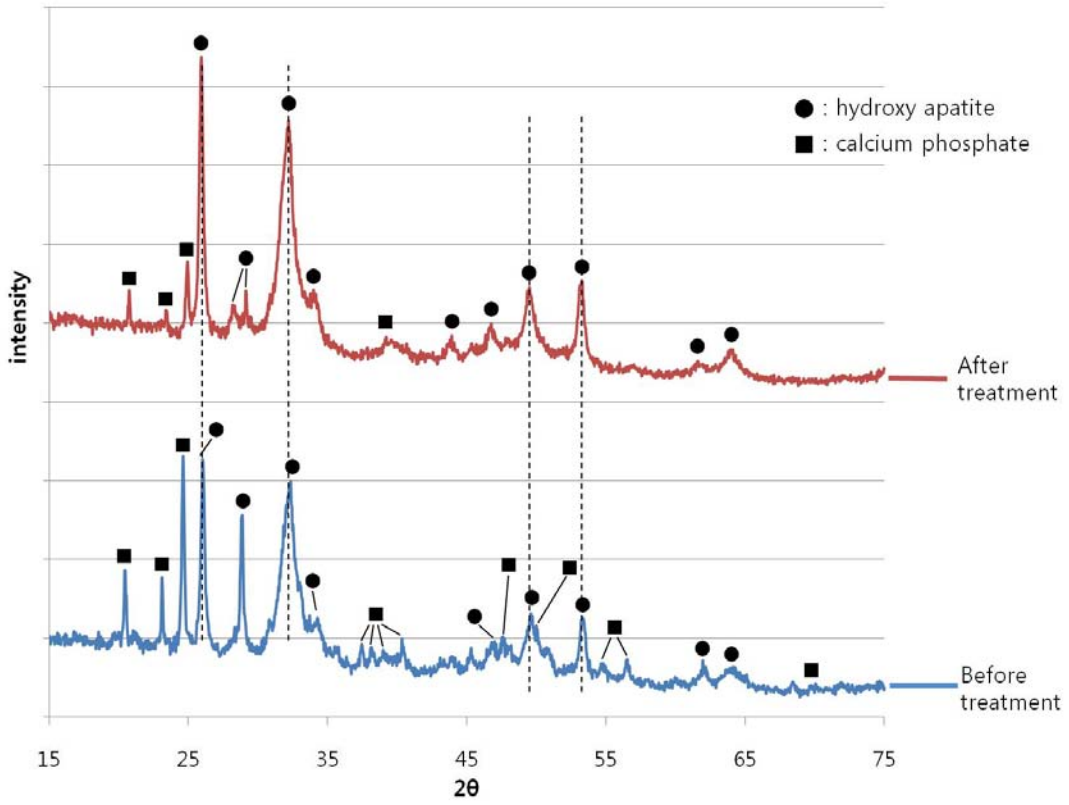

Figure 15. X-ray diffraction result of water-treated bovine bone

Figure 16 shows the XRD results of bovine bones machined for longitudinal test before and after 70%wt of isopropyl alcohol treatment for 20 minutes. The lower blue line is the result of the untreated sample XRD, and the upper red one is the isopropyl alcohol treated sample XRD data. All of the peaks in the untreated sample remained after treating except one peak located at 28.8° (2θ). The peaks located at 12.2°, 26.5°, 32.8°, 50.1° and 53.8° (2θ) were narrower and higher than the plot of untreated sample.

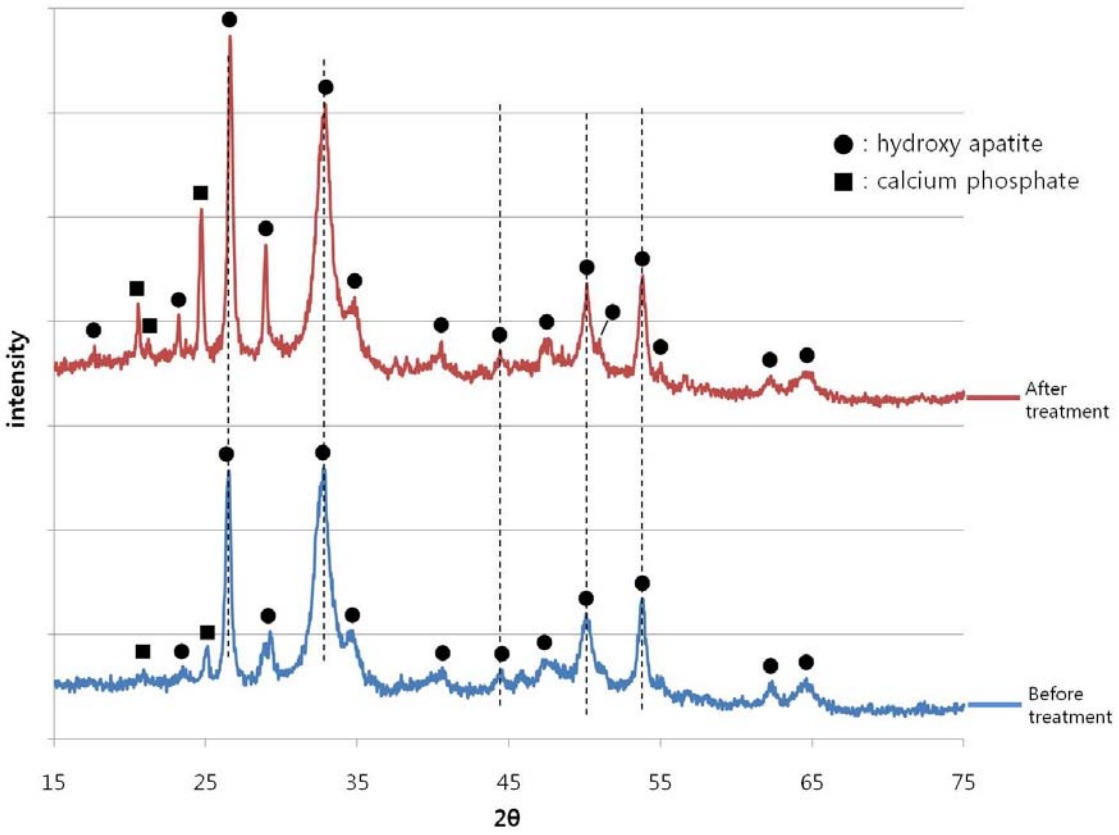

Figure 16. X-ray diffraction result of isopropyl alcohol-treated bone

Figure 17 shows the X-ray diffraction (XRD) results of before and after treated bovine bone machined for longitudinal test with the 20% wt hydrogen peroxide for 60 minutes. The lower blue plot is the results of the untreated sample XRD, and the upper red one is the hydrogen peroxide treated sample XRD data. The total shapes of two plots are approximately the same. The calcium phosphate peaks near 15°, 30° and 65° (2θ) disappeared after treatment.

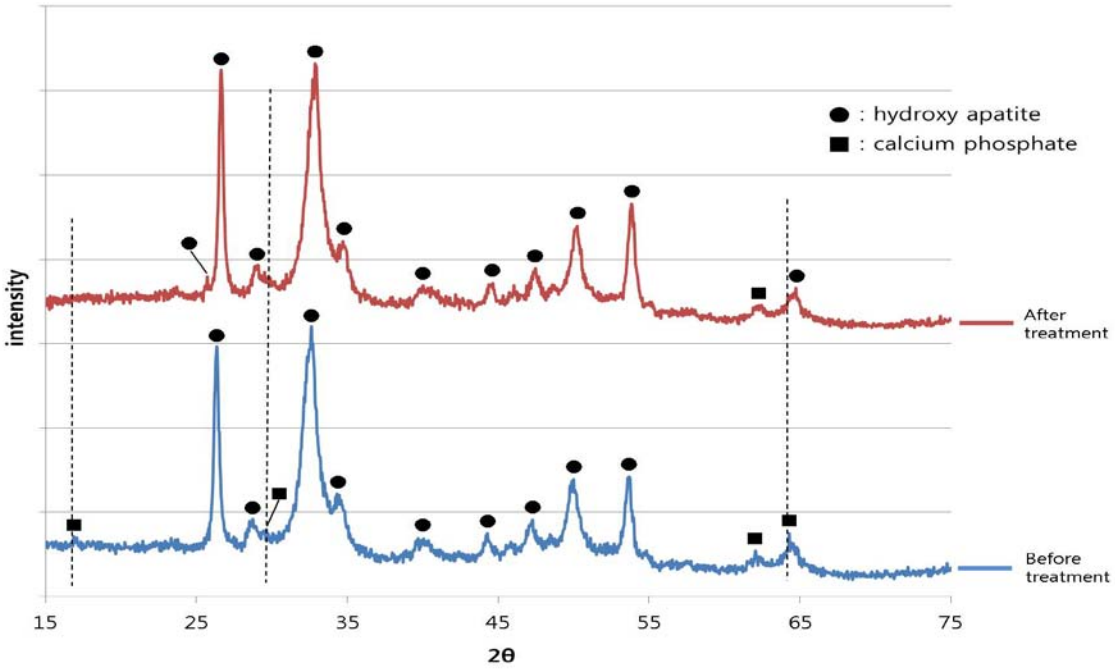

Figure 17. X-ray diffraction result of hydrogen peroxide-treated bone

4.1.2. Bacterial colony forming units

Quantifying bacteria colony forming units provides a measure of how successfully the solution cleansed the bone samples. When a bacterium can grow successfully, it forms a colony. The digital microscope VHX-600 (Keyence, Woodcliff Lake, New jersey, USA) was used to count the number of the bacterial forming colonies with a magnification of 20x.

Overall, 33 nutrient agar plates with swipes from the non-treated bone samples were incubated. Results are shown in Figure 18. After 120 hours of incubation, bacterial forming colony units were observed in most of the nutrient agar plates. Seven plates out of 33 did not contain any forming colony units, but the other 26 plates contained at least one to at most more than one hundred forming colony units.

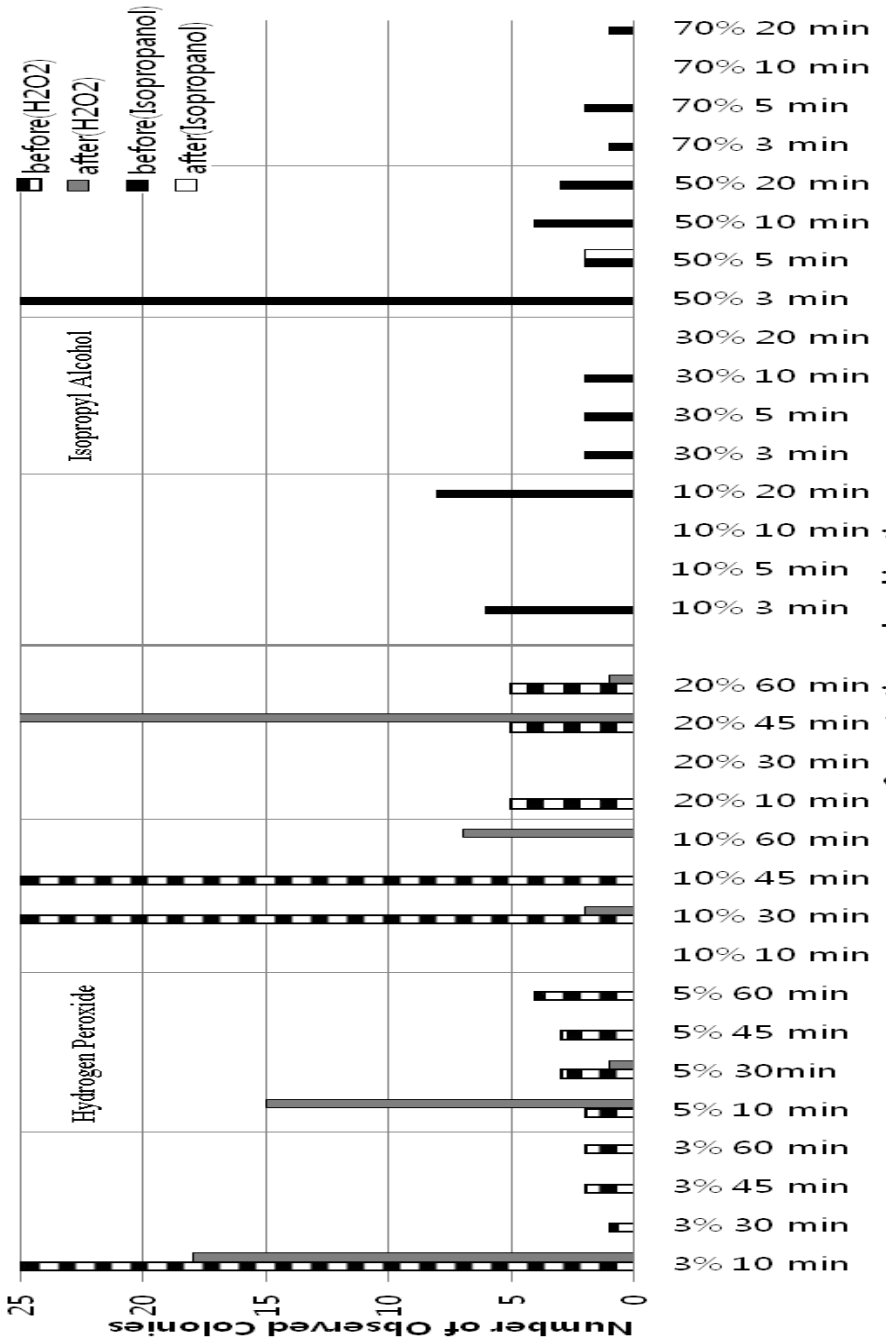

Figure 18. Number of colonies forming units detected from bovine bone samples treated with increasingly concentrated solutions of hydrogen peroxide and isopropyl alcohol for varying durations (3~20 minutes)

After treating bovine bone samples with the sixteen conditions of isopropyl alcohol, all bacteria colonies were eradiated except one plate. Twelve out of the sixteen agar plates were swiped with untreated bone samples, and they contained bacteria colonies. Fifteen out of sixteen plates were swiped with treated bone samples had no bacteria except one. That plate was swiped with the bone sample treated with 50%wt of isopropyl alcohol for 5 minutes. Moreover, the agar swiped with the untreated bone sample formed one bacteria colony and one fungal colony. However, the agar swiped with the 50%wt isopropyl alcohol treated bone sample, formed two fungal colonies. Figure 19 shows the bacterial colony counts for untreated and treated bone. A representative agar plate swiped with untreated bone samples is shown in (a), and the agar plate swiped with treated bone sample is shown in (b). All bacterial and fungal colonies on the agar plate were shown in the top and bottom inserted picture.

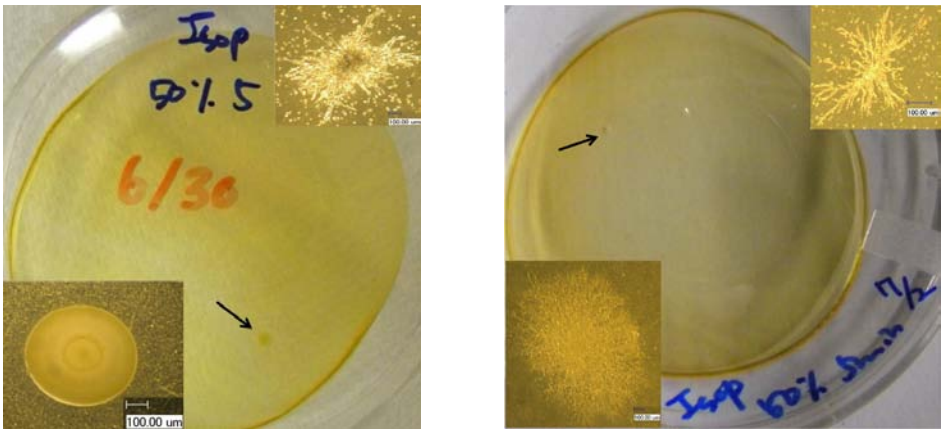

(a) (b)

Figure 19. The agar swiped with the untreated bone in (a) and the bone treated with the 50%wt isopropyl alcohol for 5 minutes in (b). (Every colony was captured in the inserted picture.)

Overall, fewer forming colony units were obtained from the bovine bone treated with hydrogen peroxide. Thirteen out of sixteen plates showed bacteria colonies in the non-treated conditions. After treatment with hydrogen peroxide, only seven out of sixteen plates contained bacteria colonies. In four out of seven plates, the number of bacteria colonies decreased after hydrogen peroxide treatment. In three plates swiped with the bone samples treated with 5%wt-10 minutes, 10%wt-60 minutes and 20%wt-45 minutes, the number of bacteria colonies increased. In the plate that was swiped with soaking in 20%wt hydrogen peroxide for 45 minutes, there were a number of bacteria along the nutrient agar edge. Figure 20 shows a number of grown bacteria colony forming units along the edge of the agar plate out of the swiped route by the cotton swabs.

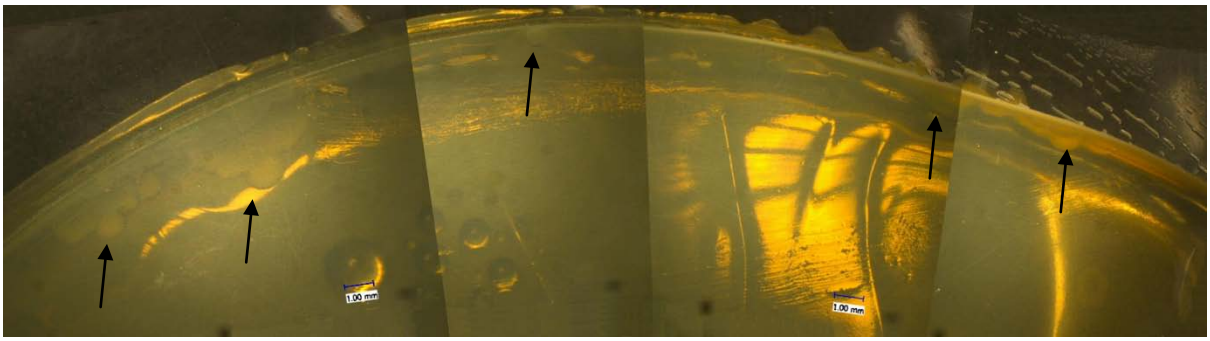

Figure 20. Grown bacteria colonies along the edge of the agar plate.

4.1.3. Small punch test results

Figure 21 shows results of the small punch test of bovine bone treated in 5%wt hydrogen peroxide for 10~60 minutes. Each plot represents the average value of 3~5 tests of each condition on separate bones. The tests stepped when the upper jig started to contact the bone samples. As the soaking time increased, the maximum endurable load decreased.

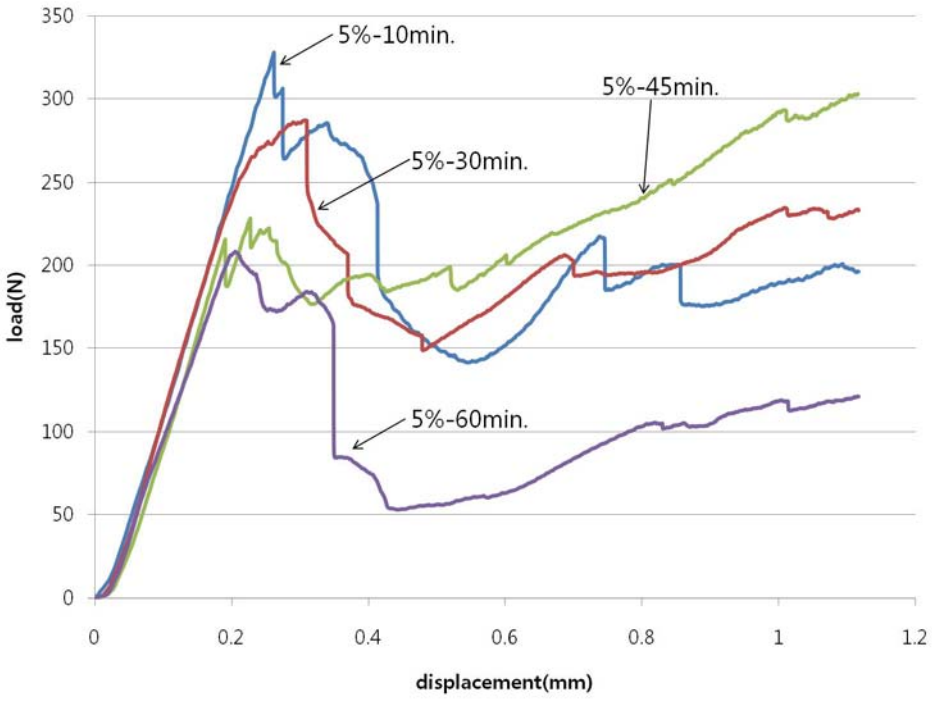

Figure 21. Representative small punch test graph of the bovine bone soaked in 5%wt H_2O_2

Figures 22 and 23 show the overall small punch test data for the hydrogen peroxide and the isopropyl alcohol treated group, and tables 4 and 5 show the values. The average

maximum endurable load for the control sample, which was untreated, is illustrated by the blue star at zero minute. Weak tendency of decreasing maximum endurable load is shown in the graph below as increasing time soaked in hydrogen peroxide. For the isopropyl alcohol treatment result, increasing and/or decreasing tendency were not observed.

Table 4. The maximum load of H_2O_2 treated bone

Condition		Average maximum load (N)	Standard deviation	Number of samples
Concentration	Soaking time			
3%	10 min.	358.7	24.1	4
3%	30 min.	320.8	11.2	3
3%	45 min.	292.2	8.3	3
3%	60 min.	334.4	8.7	5
5%	10 min.	358.2	27.5	3
5%	30 min.	338.2	57.1	4
5%	45 min.	266.2	34.1	5
5%	60 min.	256.3	1.2	3
10%	10 min.	317.3	32.1	2
10%	30 min.	264.7	2.8	3
10%	60 min.	232.5	-	1
20%	10 min.	359.3	30.7	4
20%	30 min.	297.3	36.1	4
20%	45 min.	307.8	49.9	3
20%	60 min.	269.4	36.1	3

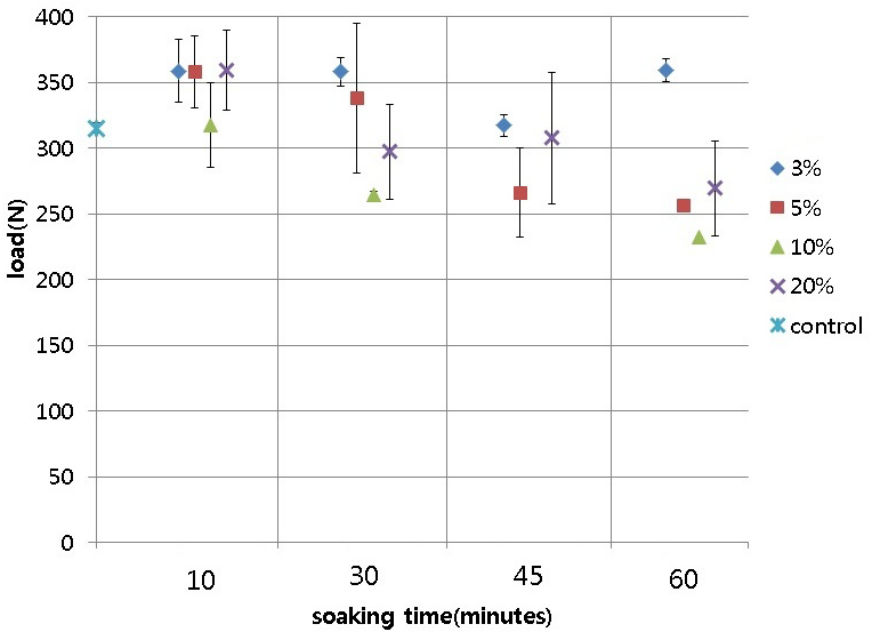

Figure 22. Small punch test results of H_2O_2 treated bovine bone treated varying concentrations of H_2O_2 for increasing time duration

Table 5. The maximum load of isopropyl alcohol treated bone

Condition		Average maximum load (N)	Standard deviation	Number of samples
Concentration	Soaking time			
10%	3 min.	362.3	3.5	4
10%	5 min.	331.7	26.5	4
10%	10 min.	260.7	76.6	4
10%	20 min.	353.8	30.6	3
30%	3 min.	367.3	3.8	3
30%	10 min.	282.0	25.2	5
30%	20 min.	387.9	11.8	3
50%	3 min.	299.3	-	1
50%	5 min.	332.3	65.5	3
50%	10 min.	343.3	35.0	3
70%	3 min.	331.7	34.4	4
70%	5 min.	336.0	9.5	4
70%	10 min.	316.4	13.8	3
70%	20 min.	315.9	42.0	4

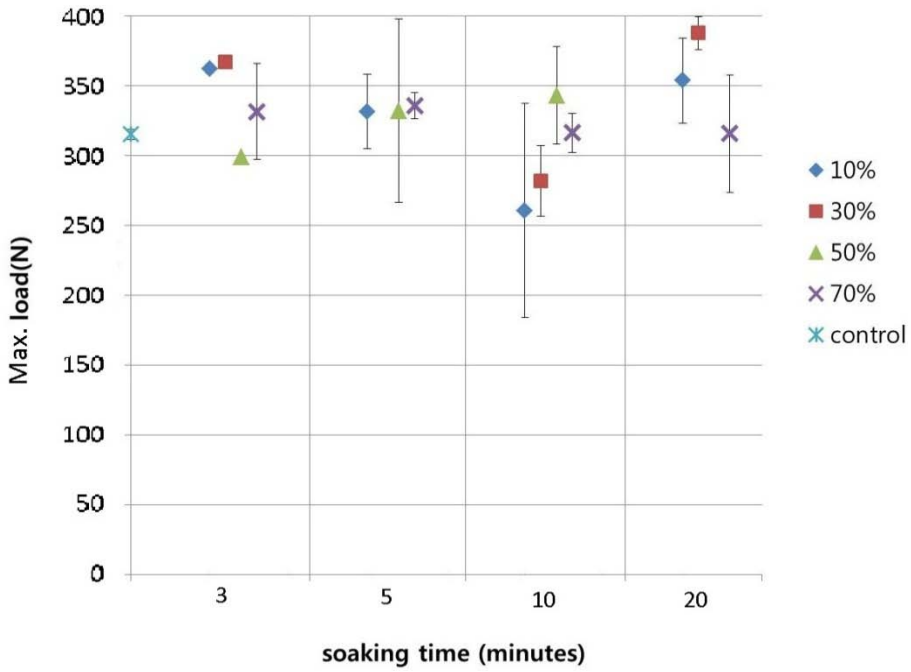

Figure 23. Small punch test results of the isopropanol treated bovine bone treated varying concentrations of H_2O_2 for increasing time duration

4.2. Mechanical properties of bovine and human bone

4.2.1. Bovine bone

The small punch test was used for studying mechanical properties of the bovine bone. Along the longitudinal direction, the elastic modulus was the highest, while it was lowest in the radial direction. Table 6 shows the elastic modulus of each directional test on the bovine femur, and figure 24 shows that in the bar graph.

Table 6. The mechanical properties of the three directional bovine femurs

Direction	Elastic modulus	Standard deviation	Number of samples
Longitudinal	22.3 GPa	2.3	9
Radial	13.9 GPa	1.6	6
Circumferential	17.2 GPa	2.0	5

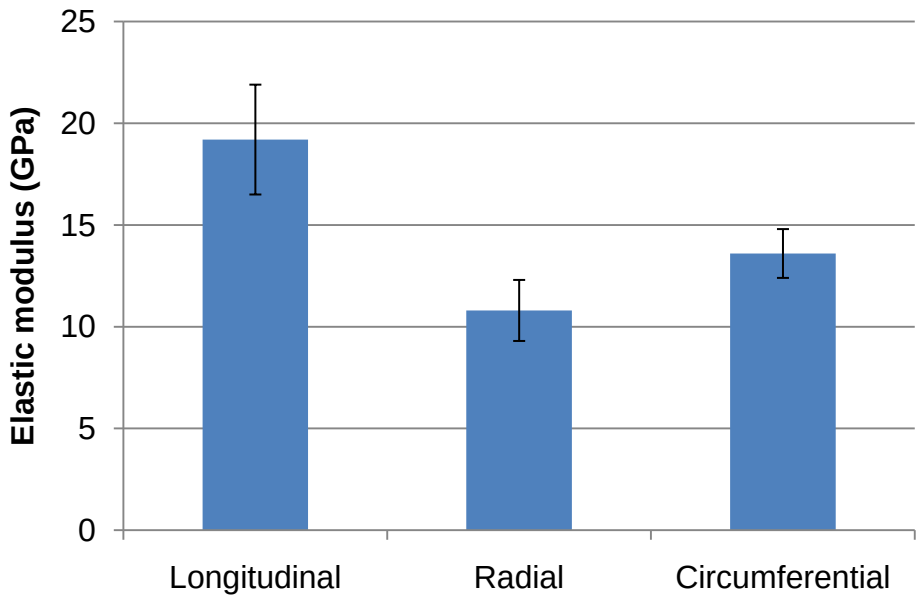

Figure 24. The elastic moduli of the bovine bones machined in three different direction

4.2.2. Failure analysis of bovine bones

When the small punch test was applied to a workpiece material, the 1mm diameter ball bearing indented through the sample. The fractography of the bovine bone by the ball bearing was then observed. Figure 25 shows the optical microscopic images of the fractured surface of bovine bone samples machine for longitudinal test. The fractured surface obtained

under the increasing load is shown in (a). The fractured surface under the stable load is shown in (b). The fractured surface obtained under a decreasing load is shown in (c). That obtained when the upper jig being contacted is shown in (d). A portion of the sample under the ball bearing was pushed out by the ball bearing. Figure 26 shows the result of small punch test in the condition similar to (d). When the small punch test ran for a long time, the rod is in contact with the upper jig, and the upper jig started to press the sample. This is the reason why on the plot there is a sudden increase.

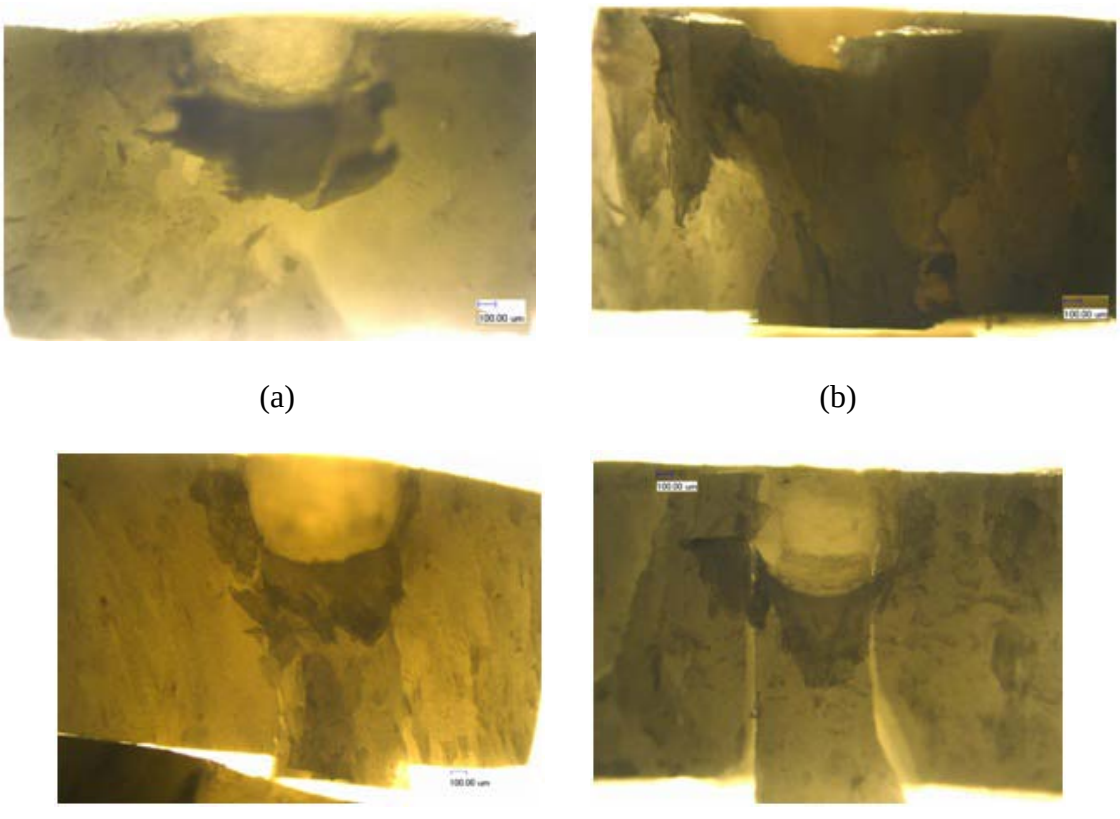

(a) (b)

(c) (d)

Figure 25. Side-views of small punch tested bovine bone machined perpendicular to longitudinal direction

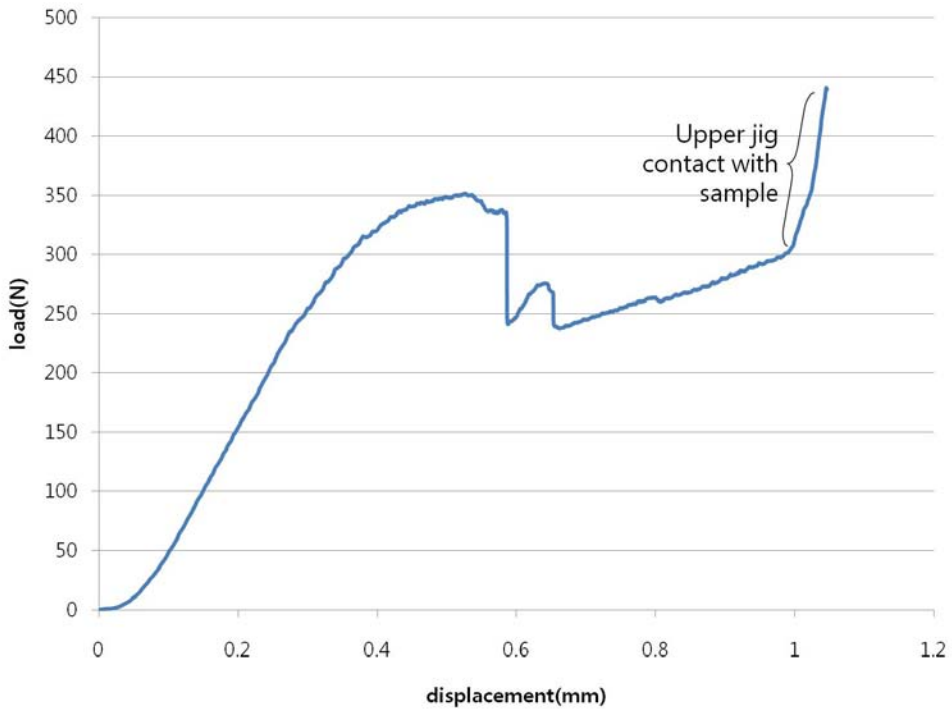

Figure 26. Small punch test result of Figure 25-(d)

Figure 27 shows the optical microscopic images of the radially pushed and fractured bovine bone samples. When the small punch test was conducted on the bovine bone samples machined for radial test, the region under the ball bearing was cracked instead of being pushed out. The fractured surface obtained during an increasing load is shown in (a). The fractured surface obtained after second fracture is shown in (b). The fractured surface obtained during stable load is shown in (c). The fractured surface obtained during the upper jig contacted the sample is shown in (d). Figure 28 shows the small punch test of the bone samples in the figure 27-(d).

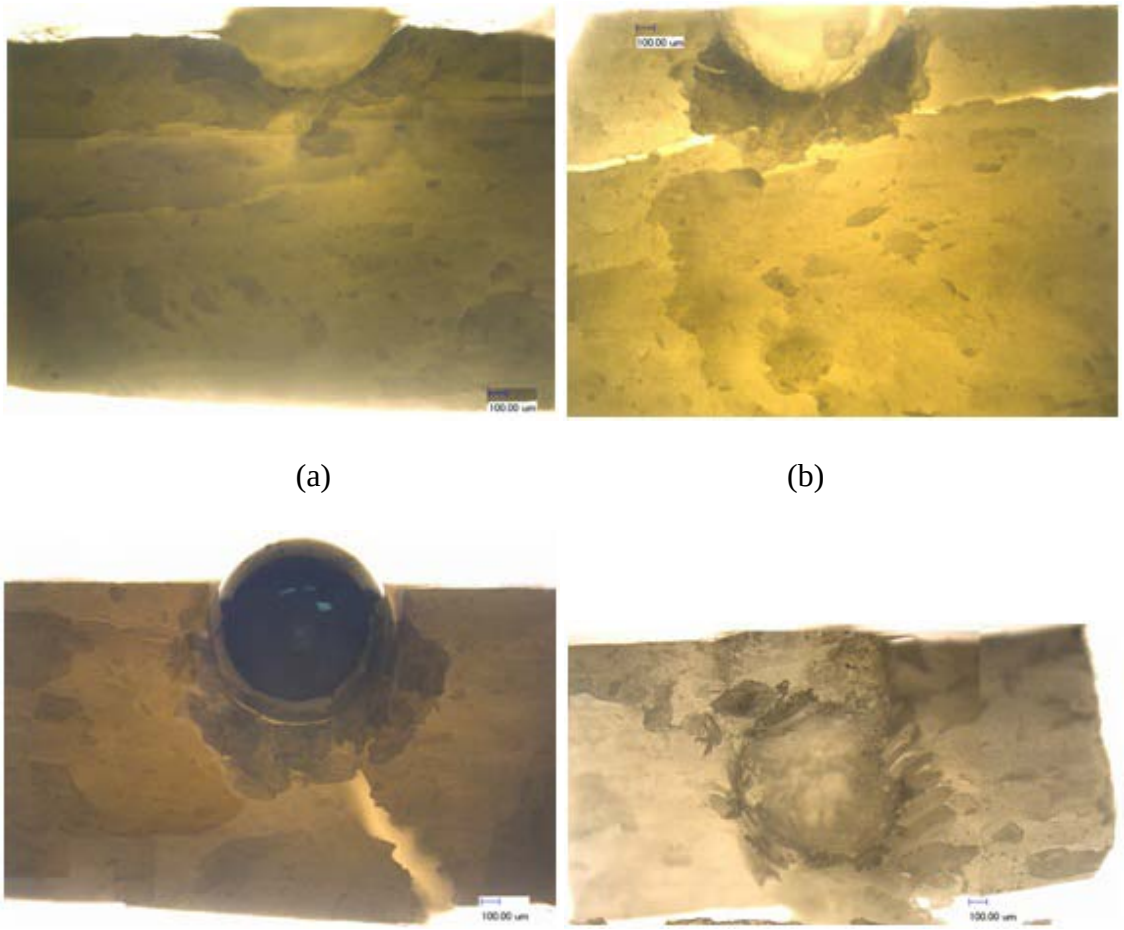

(a) (b)

(c) (d)

Figure 27. Side-views of the small punch tested bovine bone machine on the x-z and y-z plane direction

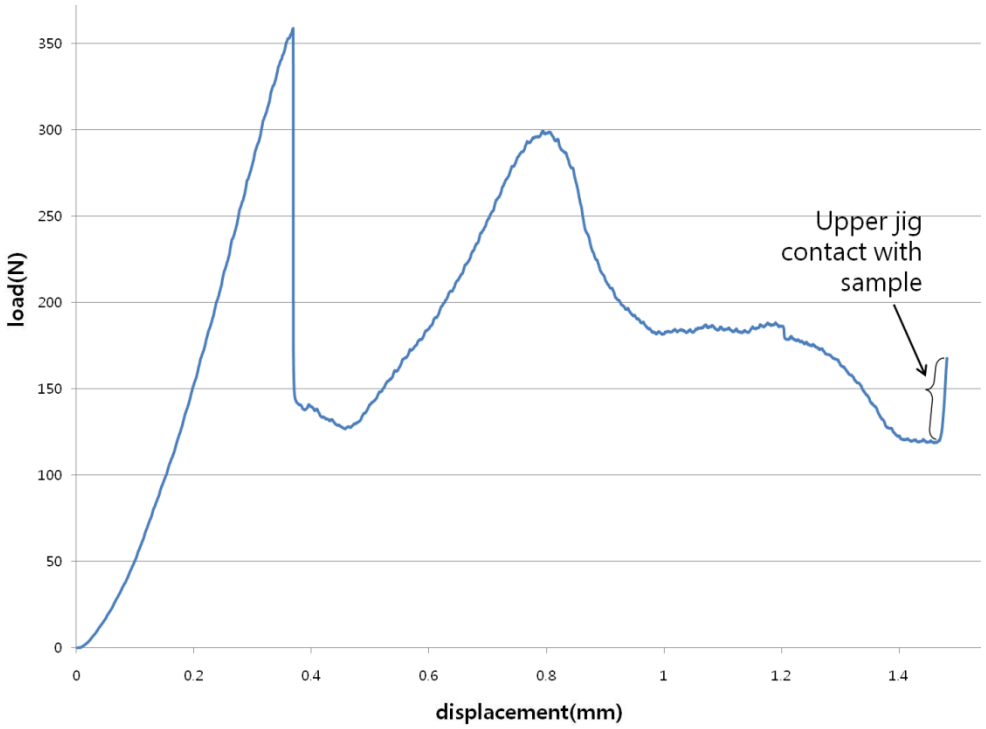

Figure 28. The small punch test result of the bone sample in the figure 27-(d)

Figure 29 shows the optical microscopic images of the fractured surfaces of the bovine bone samples machine along radial direction. The fractured surfaces of the circumferentially tested bone samples were similar to the radially tested bone samples. The optical microscopic (OM) image of fractured surface obtained right after the highest sustainable load is shown in (a). The OM image of fractured surface obtained under increasing load is shown in (b). The OM image of fractured surface obtained under stable load is shown in (c). The OM image of fractured surface obtained during decreasing load is shown in (d). The SEM images of the same fracture surface to the figure 29-(d) in magnification of 68x and 300x are shown in (e) and (f).

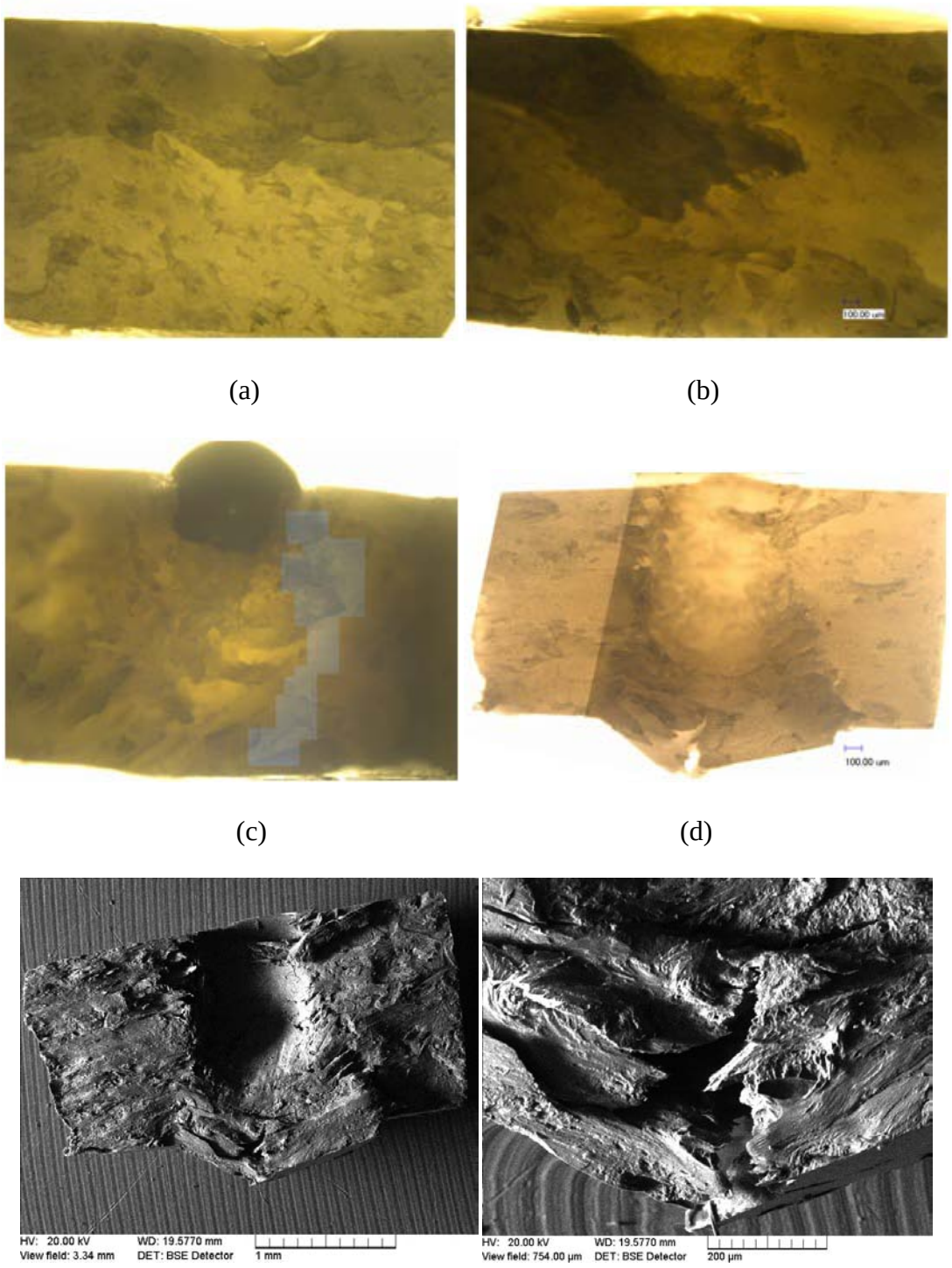

Figure 29. Side-views of the small punch tested bovine bone machined for circumferential test

4.3. Effects of infiltrated tumor on the human bone

4.3.1. Properties of the human bone

To study the effect of cancer cells, the density of bones was measured. Subsequently, the small punch test was conducted, and microscopic observation was performed. Table 7 shows the volume densities and the elastic modulus of the tumor-free human bone and the cancerous human bone. The density of cancerous bone was 25% less than the tumor-free bone. The elastic modulus of the cancerous bone was 99% less than that of a tumor-free bone. Figure 30 shows the microscopic images of the fractured surfaces of the tumor-free human bone. As shown in Figure 30, the portion under the ball bearing was pushed out in the longitudinally tested human bone sample, and the fractured surfaces were similar to the longitudinally tested bovine bone samples. The fractured surface obtained under increasing load is shown in (a). The fractured surface obtained under decreasing load is shown in (b). The fractured surface obtained under stable load is shown in (c). The fractured surface obtained during the upper jig contacted the sample is shown in (d). The SEM images of the same fractured surface to the figure 30-(d) in magnification of 78x and 250x are shown in Figures 30-(e) and (f).

Table 7. The density and elastic modulus of human bones

Classification	Density	Standard deviation	Elastic modulus	Standard deviation	Number of samples
Tumor-free	$1.6x10^{-3}g/mm^3$	0.1	20.0GPa	1.8	9
Cancerous	$1.2x10^{-3}g/mm^3$	0.1	0.3GPa	0.06	6

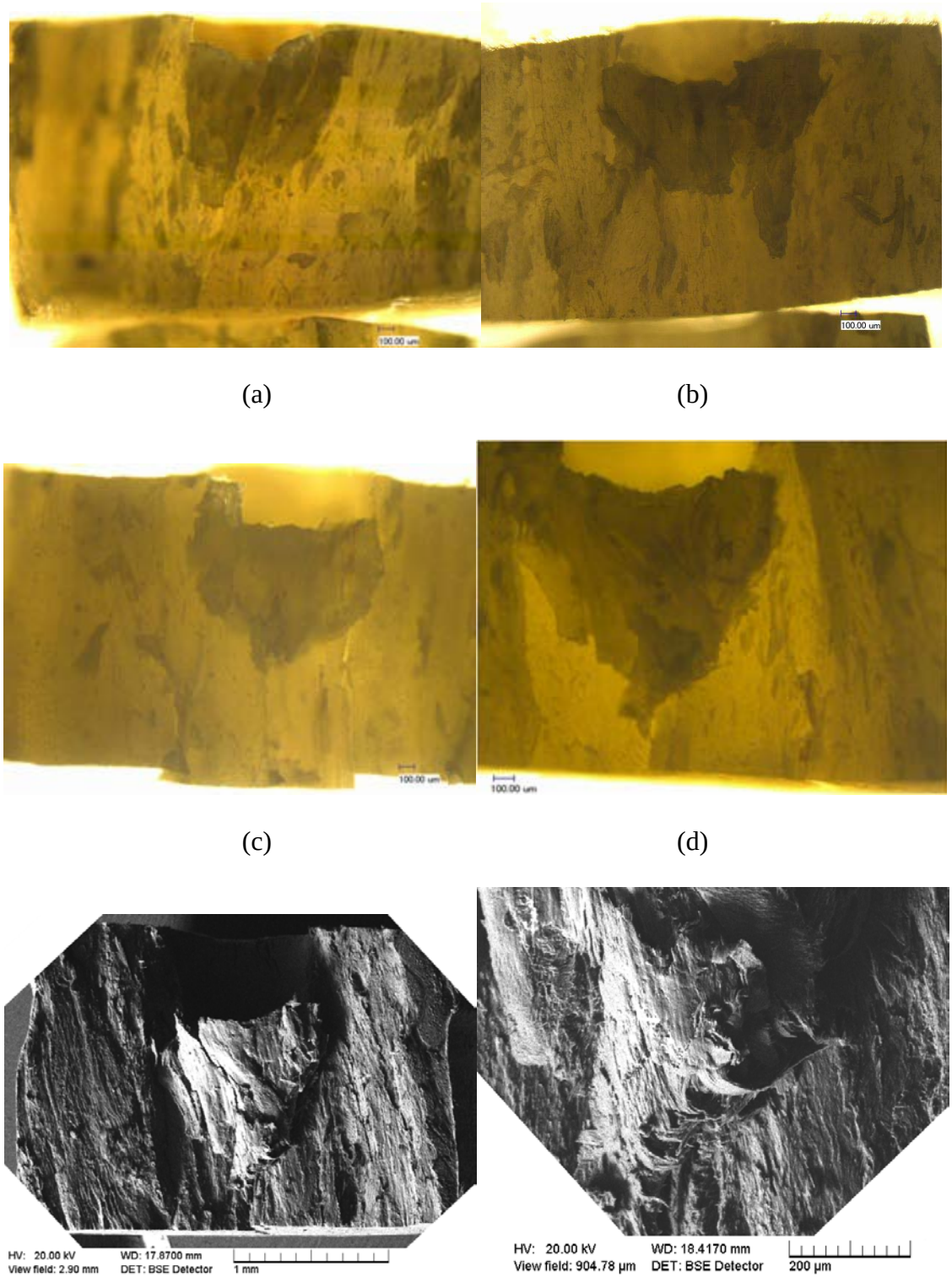

(a) (b)

(c) (d)

(e) (f)

Figure 30. Fractured surfaces of the small punch tested tumor-free human tibia

The cancerous bones were severely damaged after SPT and there was no visible built up of the compressed bones. This means that the diseased bone was highly porous and the resistance to penetration was minimal. Figure 31 shows the optical microscope (OM) and the scanning electron microscopic (SEM) images of cancerous bone. The side-view of OM image of the tested cancerous bone is shown in (a). The bottom-view of the OM image on tested cancerous bone is shown in (b). The SEM image of tested cancerous bone is shown in (c).

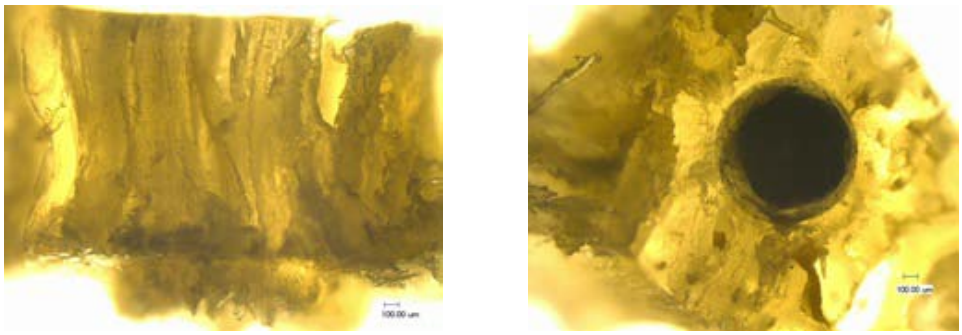

(a) (b)

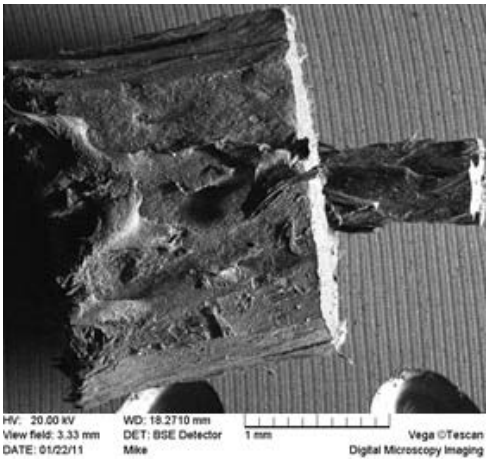

(c)

Figure 31. Optical microscope images and SEM image of tested cancerous bone

4.3.2. Comparing with a synthetic material

In order to develop synthetic materials to replace bones, comparison of their properties with those of human bones were done using small punch test. Table 8 shows the measured displacement of the synthetic material and the bovine femur when the load was the greatest during elastic behavior. Figure 32 shows the displacement of the materials measured by the small punch test as a bar chart. Table 9 shows the calculated slope of the small punch test on the synthetic material, the tumor-free human bone and the cancerous human bone. Figure 33 shows the measure slope of the cancerous bone and the synthetic material in bar chart. The displacement of the cancerous bone at the maximum load had the largest value, and the synthetic material had the second. However, the two values are quite similar, so that the ranges of the standard deviations were overlapped. The slope of the small punch test on the synthetic materials was two times higher than that of the cancerous human bone.

Table 8. The measured displacement at the maximum load

Material		Displacement	Standard deviation	Number of samples
Synthetic material		0.66mm	0.08	11
Bovine femur	Longitudinally tested	0.28mm	0.03	10
	Radially tested	0.44mm	0.15	7
	Circumferentially tested	0.38mm	0.16	9
Human bone	Tumor-free bone	0.36mm	0.05	9
	Cancerous bone	0.80mm	0.11	6

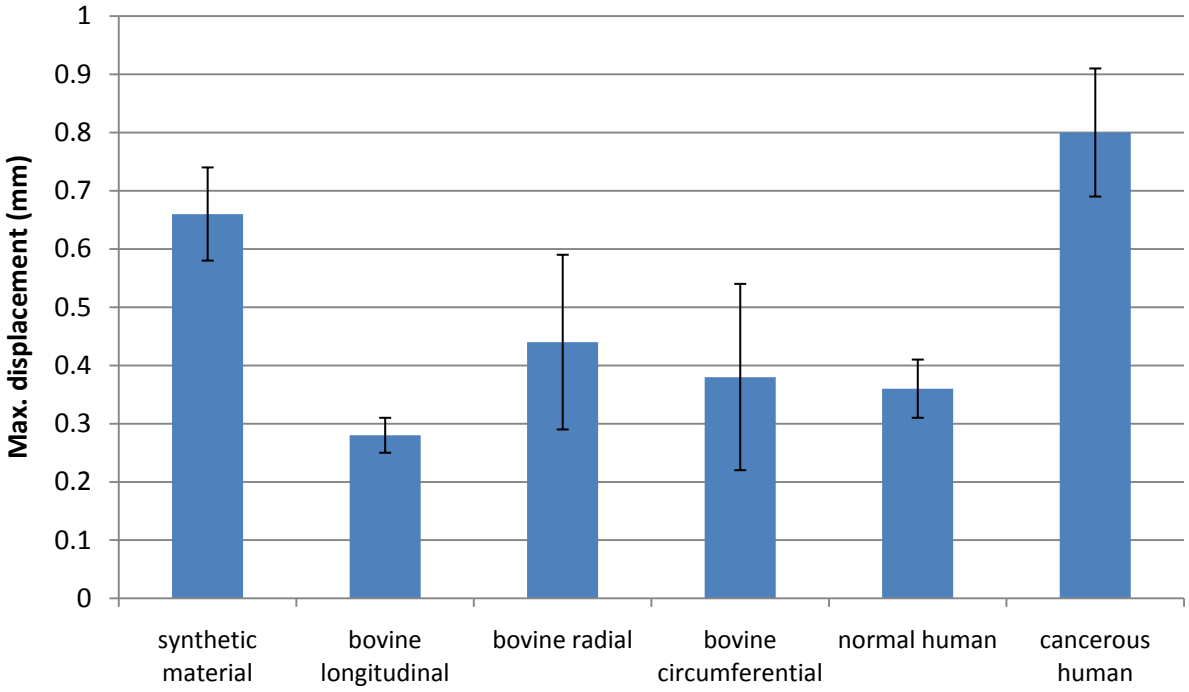

Figure 32. Measured displacement under the maximum load of the materials

Table 9. The calculated plot slope of the small punch test

Material	Slope	Standard deviation	Number of samples
Synthetic material	28.0N/mm	5.4	11
Tumor-free human bone	684.4N/mm	169.5	9
Cancerous human bone	14.1N/mm	4.2	6

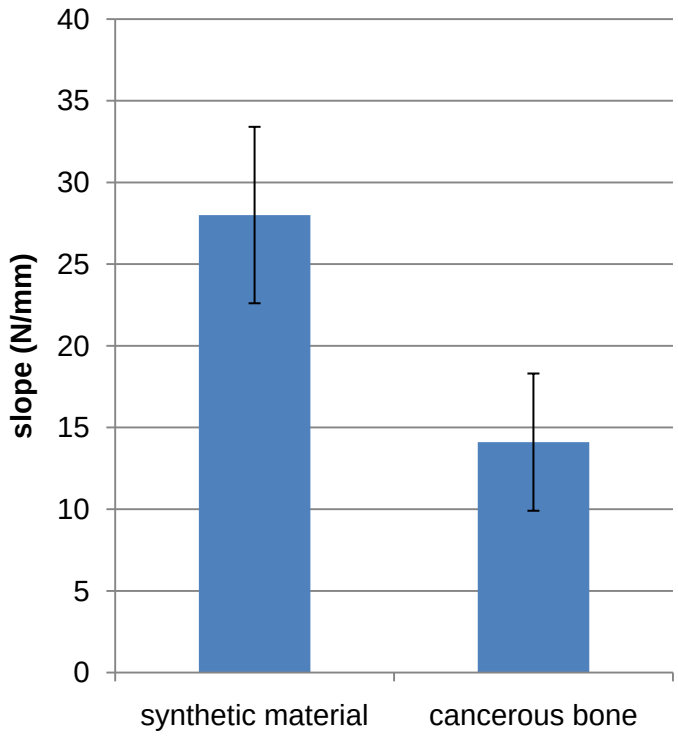

Figure 33. Measured slope during the small punch test of the synthetic material and cancerous bone

Figure 34 shows the microscopic images of the small punch tested synthetic material. The synthetic material was not fractured after the small punch test. The side view obtained at the displacement of 0.64 mm is shown in (a). The side view obtained at the displacement of 0.73 mm is shown in (b). The side view obtained during the upper jig contacted the sample is shown in (c). The side view obtained at the displacement of 0.04 mm after upper jig contacted the sample is shown in (d). The white arrow indicates the pressed portion by the upper jig.

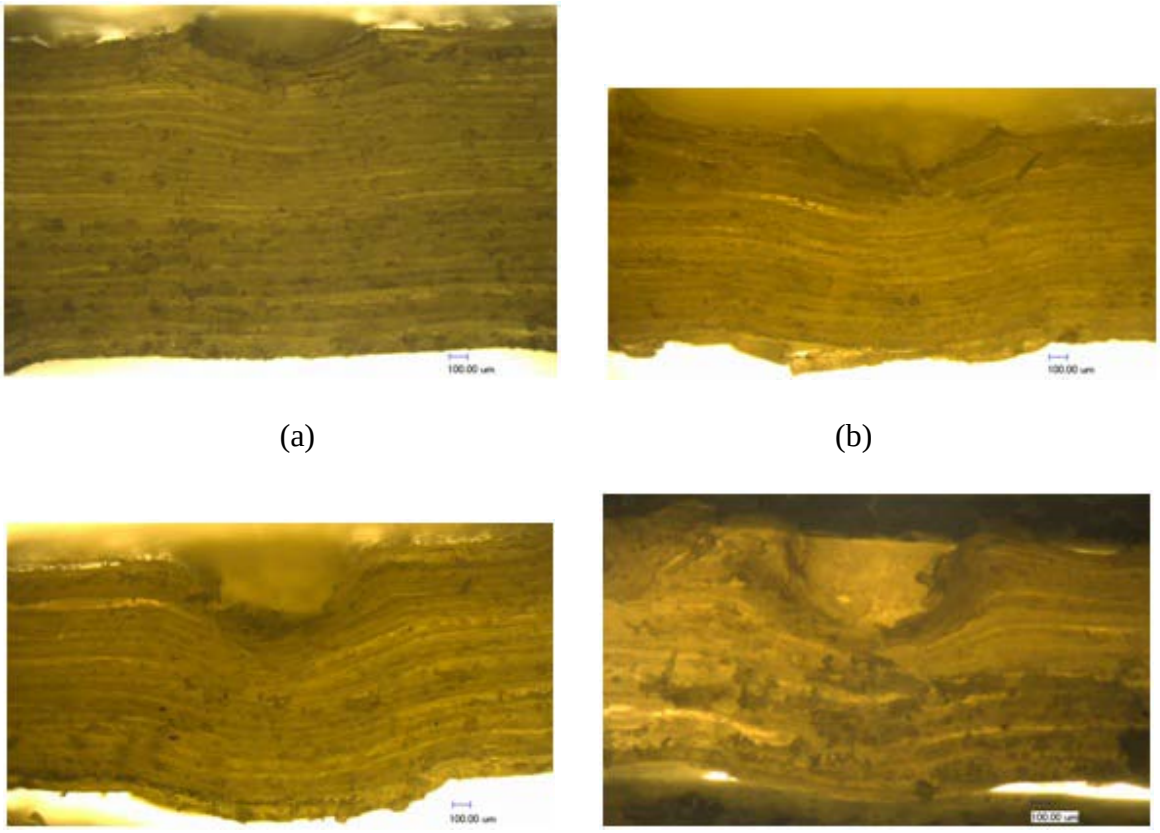

(a) (b)

(c) (d)

Figure 34. Side-views of the small punch tested synthetic material

When the small punch test was conducted on the synthetic material that was attached on the bovine bone, the maximum load and displacement were 16~36% higher than the bovine bone. Table 10 shows the maximum endurable load values with the number of samples. Figure 35 shows the microscopic images of the fractured surfaces of the synthetic material attached on the bovine bone. The top view of the small punch tested samples is shown in (a). The bottom view of the tested sample is shown in (b). The fractured surface obtained right after second fracture is shown in (c). The fractured surface obtained during the upper jig contacted the sample is shown in (d).

Table 10. Maximum endurable load of bovine bone and synthetic material on the bovine bone

Material		Maximum load	Standard deviation	Number of samples
Bovine bone	Longitudinal	313.5N	38.4	10
	Radial	346.4N	56.5	7
Synthetic material on the bovine bone	Longitudinal	363.3N	74.3	8
	Radial	472.1N	95.6	6

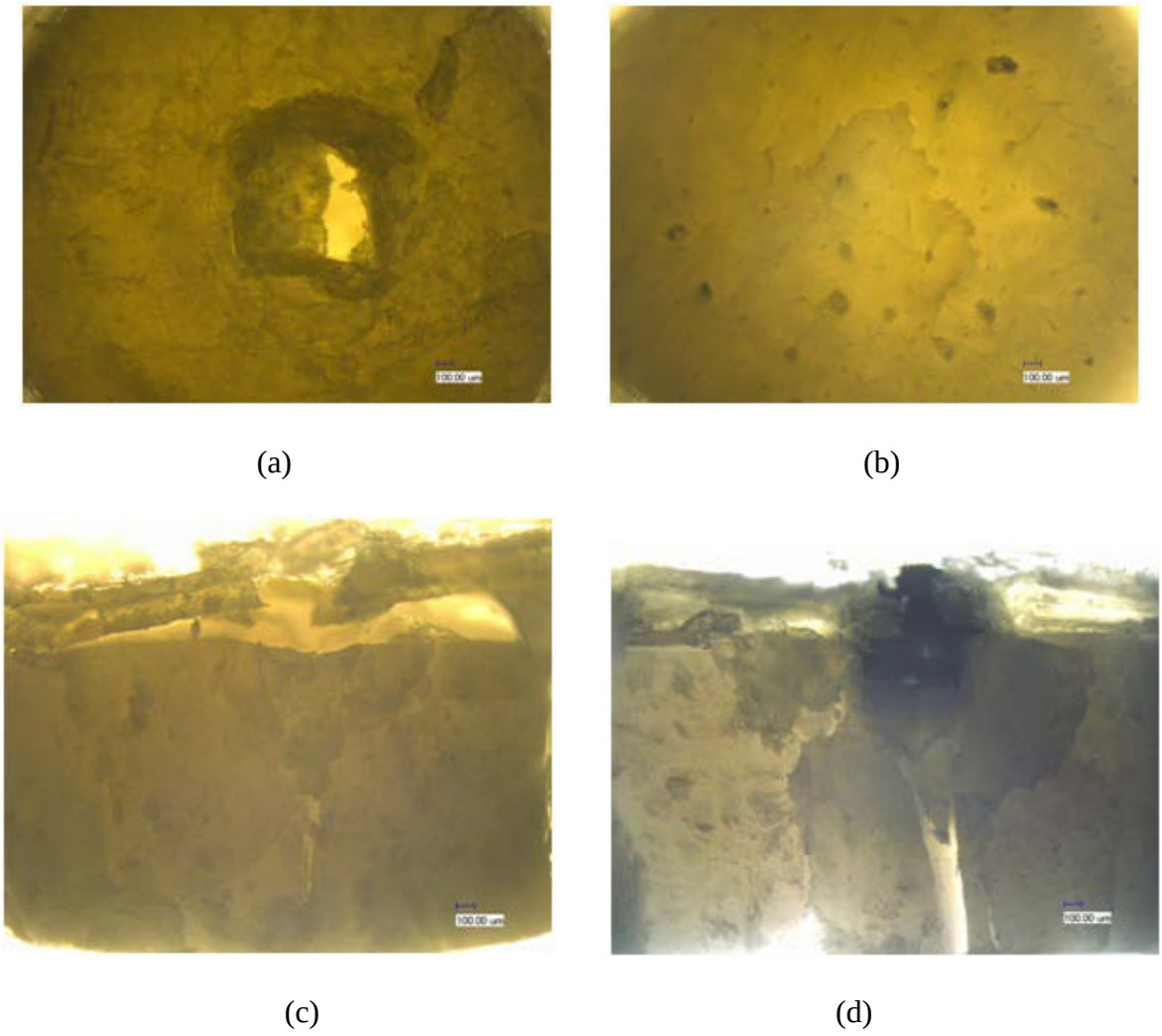

(a) (b)

(c) (d)

Figure 35. Top, bottom and side-views of small punch tested synthetic material

CHAPTER V

STRUCTURE-PROPERTY RELATIONSHIP OF BIOLOGICAL AND SYNTHETIC BIOMATERIALS

This chapter discusses the relationships between microstructure and mechanical properties of the bovine and the human bone based on results described in the previous chapter. The following subsections will provide a discussion of the effects of chemical solutions on the mechanical properties and the microstructures of the bovine bone. Discussion of the structures of directionally tested bovine bone, differences between human tumor-free and cancerous bone, and the comparative properties of synthetic material will be also presented.

5.1. Effects of chemical solution on biological materials

5.1.1. Microstructure and cleaning methods

As shown in the figure 15, 16 and 17, no major difference existed in the XRD results between the untreated bone and the isopropyl alcohol and the hydrogen peroxide treated bones. This suggests the isopropyl alcohol and the hydrogen peroxide did not affect the microstructure of the bovine bones. For the water treated bone, the untreated bone showed, as the lower curve in Figure 15 indicates, that calcium phosphate exists (filled square). After water treatment, that amount of the calcium phosphate was reduced, and instead, the amount of hydroxyl apatite ($Ca_5(PO_4)_3(OH)$) dominated. According to Termine and Posner, [68] calcium phosphate converted into crystalline hydroxyl apatite when the bone was soaked in water so that the bone sample treated with water had a more crystalline structure [68]. The

hydroxyl apatite crystal in bone is finely divided because this mineral is formed from solution. At room temperature and under atmospheric pressure, forming a large single hydroxyl apatite crystal is impossible [69]. The width of peaks decreased as the size of hydroxyl apatite crystal increased, making the peaks narrow [69].

Concerning the cleansing effect of the chemical solutions, hydrogen peroxide and isopropyl alcohol were quite effective. On the nutrient agar plate that was swiped with the bone samples soaked in the 3%wt of hydrogen peroxide for 10 minutes, only 20% of bacterial colony units were reduced compared to the agar plate swiped with the untreated sample. Thus, the treatment with the 3%wt hydrogen peroxide for 10 minutes was not strong enough to decontaminate the bone sample. Only three out of sixteen samples treated with hydrogen peroxide demonstrated an increased number of bacteria colony forming units. However, the bacteria grew along the outer edge of the nutrient agar plate rather than along the swiped route. Thus, the increasing bacteria colony forming units were most likely formed by the bacteria from the air contamination when the lid of the petri-dish was opened. In the isopropyl alcohol group, only 50% isopropyl alcohol-5minutes treated sample had the same number of bacteria as the untreated sample. However, the sort of colony unit was different. The untreated sample had two bacterial colonies, but the treated sample had one bacterial colony and one fungal colony. Thus, the fungal colony was assumed to come from the air contamination.

5.1.2. Mechanical properties

As shown in the figure 21, the value of the load increased until a maximum loading value was reached and subsequently descended. This means that the ball bearing needed increasing load to proceed through the bone sample, and the bone subsequently fractured.

Even though the bone sample was fractured, the bone sample was held by the jig, thus the ball bearing needed a load to penetrate the gap between the fractured bone pieces. The gap between the fractured bone samples was smaller than the diameter of the ball bearing.

The maximum loading value of the highest peak before bone failure was chosen because it is a measured value of how much load a bone sample can endure before failure. Between 1) the control bone sample and the hydrogen peroxide treated samples, 2) the control bone sample and the isopropyl alcohol treated samples, it is important to determine how the maximum endurable load changed. When the standard deviations of each value from different conditions of chemical solutions were compared, the average maximum load of most samples was close to that of the control sample. Because the majority of the average values of the treated samples remained similar to the standard deviation range of the control group, this suggests that the measured average maximum endurable load values of the hydrogen peroxide and the isopropyl alcohol treated samples are not drastically different than the control sample. Therefore, it appears that the hydrogen peroxide and the isopropyl alcohol at the tested concentrations and soaking times may not be greatly altering the maximum load before the bone fractures.

5.2. Failure mechanisms of biological and synthetic biomaterials

5.2.1. Longitudinal direction

The fibrous components in the bone were arranged along the longitudinal direction. When the small punch test was finished, one dislodged grouping of fibrous components was observed. Moreover, the samples were separated into two or three pieces because of the penetration by the ball bearing. Figure 36 shows the longitudinally machined bone behavior

of the small punch test. At first, the ball bearing was adjusted on the sample surface. Then the elastic penetration occurred and the portion of the sample contacting with the ball bearing was squashed [63]. After the elastic penetration, the sample obtained cracks, and the portion of the sample in contact with the ball bearing was pushed out. Figure 30-(e) and (f) showed the torn portion of human bone machined for longitudinal test. When the portion was pushed out, the side face of the fibrous components was torn from the whole sample. This mechanism allows the bone to be stronger and tougher in the axial direction.

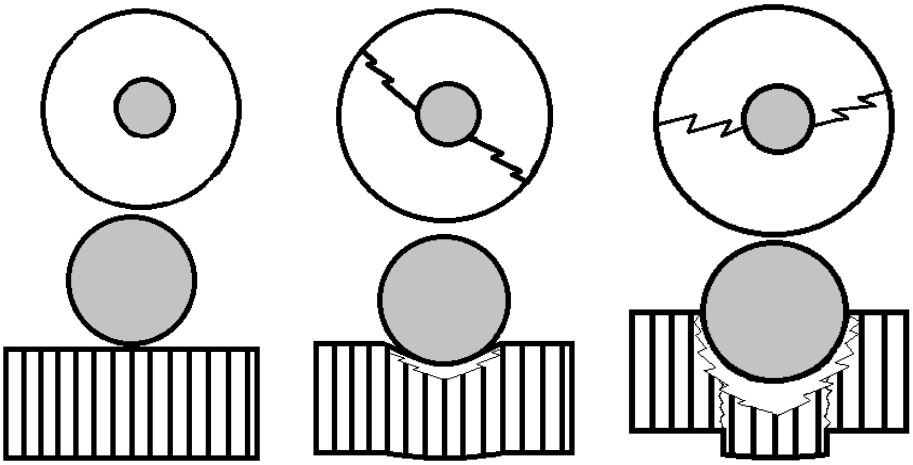

Figure 36. Top view and side view of tangentially machined bone behavior during the small punch test

5.2.2. Tangential direction

The small punch test was then conducted tumor-free to the fibrous components. Thus, the behavior of the structure of the sample was different from the longitudinal test. In this test on tangentially machined bone, the fibrous components were broken rather than pushed out.

Figure 29-(e) and (f) showed the broken bovine bone. Figure 37 shows the stages of the bone sample behavior of the small punch test. The figure 37-(a) shows the adjusted ball bearing on the bone sample surface. Inducing a crack in the sample is shown in (b). Breaking of the horizontal fibrous components is shown in (c). Failure on the bottom of the sample is shown in (d). During these stages, squashing by the ball bearing on the sample occurred. This mechanism is considered more brittle than longitudinal failure mechanism.

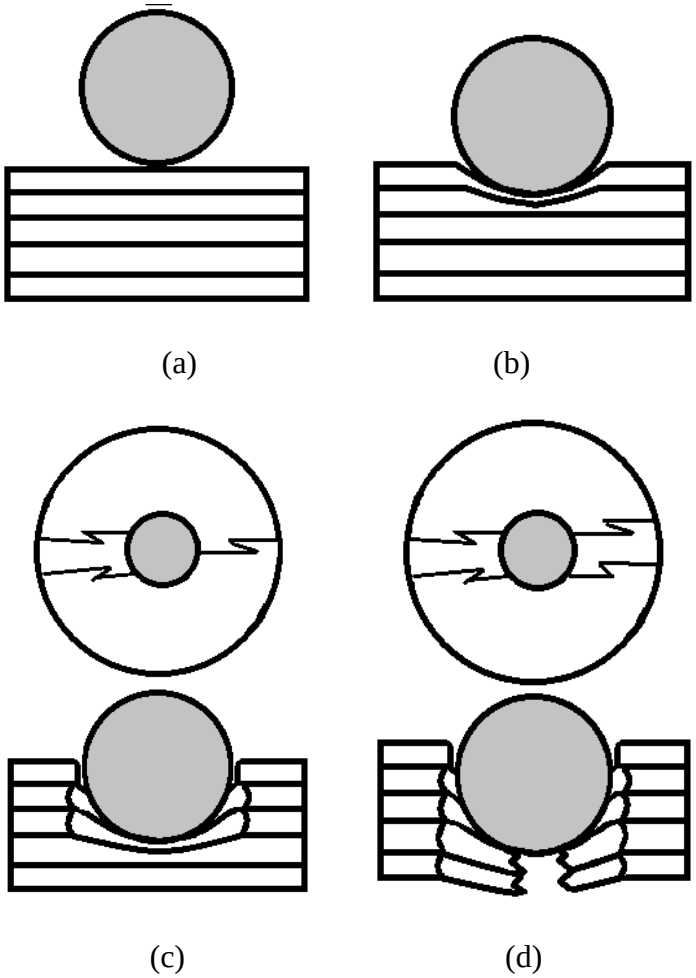

Figure 37. Top view and side view of the bovine bone axially machined behavior during the small punch test

5.2.3. Human bone

The result of the small punch test on the tumor-free human bone was similar to the longitudinally tested bovine bone because the small punch test conducted along the axial direction in the tumor-free human bone. As shown in the figure 30-(e) and (f), a torn portion of bone was observed. Combined fibers tore while undergoing a longitudinal load. The higher elastic modulus via the axial direction is obtained by this method.

The negative effect that cancer cells have on the bone was observed in the density measurement and the small punch test. The percentage of bone's crystallinity depends on age, disease and diet [69]. According to Kate et al., the bone infected by Ewing's sarcoma had 62% less bone mineral density [70]. Moreover, less dense bone has lower elastic modulus; J.D. Currey discovered that porosity and elastic modulus have a reciprocal relationship [71]. Schaffler and Burr discovered that the volume fraction versus elastic modulus have a 10.92 power of the linear logarithmic relationship, and apparent density versus elastic modulus have a 7.4 power of the linear logarithmic relationship [72]. The relationship of these human bone specimens is shown in equation (2). The apparent density of the human bone samples were represented as ρ_a. According to this relationship, the elastic modulus of cancerous bone is 1.2 GPa, six times higher than measured modulus. Thus, the cancerous bone was affected in more factors than the density.

$$E = 0.65\rho_a^{7.4} \qquad (2)$$

5.2.4. Synthetic materials

The small punch test was conducted on the layer-by-layer synthetic material. During the small punch test on the synthetic material attached to the bone, the synthetic material wrapped around the ball bearing. Thus, the tip of the ball bearing became blunt, the cross section area became larger, and the maximum sustainable load became larger as well. Figure 38 shows the stages of the small punch test on the synthetic material attached to the bone. Complete contacting between the ball bearing and sample is shown in the figure 38-(a). Squashing and wrapping mechanism of the synthetic material is shown in the figure 38-(b). Figure 38-(c) shows that the wrapped and blunt ball bearing starts to push the bone. Figure 38-(d) and (e) shows the fractured bone part in the top-view and that the region of the synthetic material under the ball bearing is completely separated and the portion of the bone under the ball bearing was separated and pushed out.

5.3. Mechanical properties

5.3.1. Elastic modulus

The elastic moduli of human bone and bovine bone have been calculated by many methods [23, 71, 73-78]. As compared with the elastic moduli from other methods, the calculated elastic modulus by the small punch test measurement was fairly rational. The measured elastic modulus by the small punch test was 22.34 GPa on the longitudinal direction, 13.91 GPa on the radial direction and 17.19 GPa on the circumferential direction. The elastic moduli from other methods are 18.2~24.4 GPa on the longitudinal direction and 11.7 GPa on the tangential direction. For the elastic modulus of human bone, the small punch test obtained the value of 21.1 GPa, and other methods obtained 17.4~25.1 GPa. Tables 11

and 12 show the elastic moduli from other methods. Tables 11 and 12 shows the elastic moduli of bovine femur and human tibia, and the numbers in brackets are standard deviations.

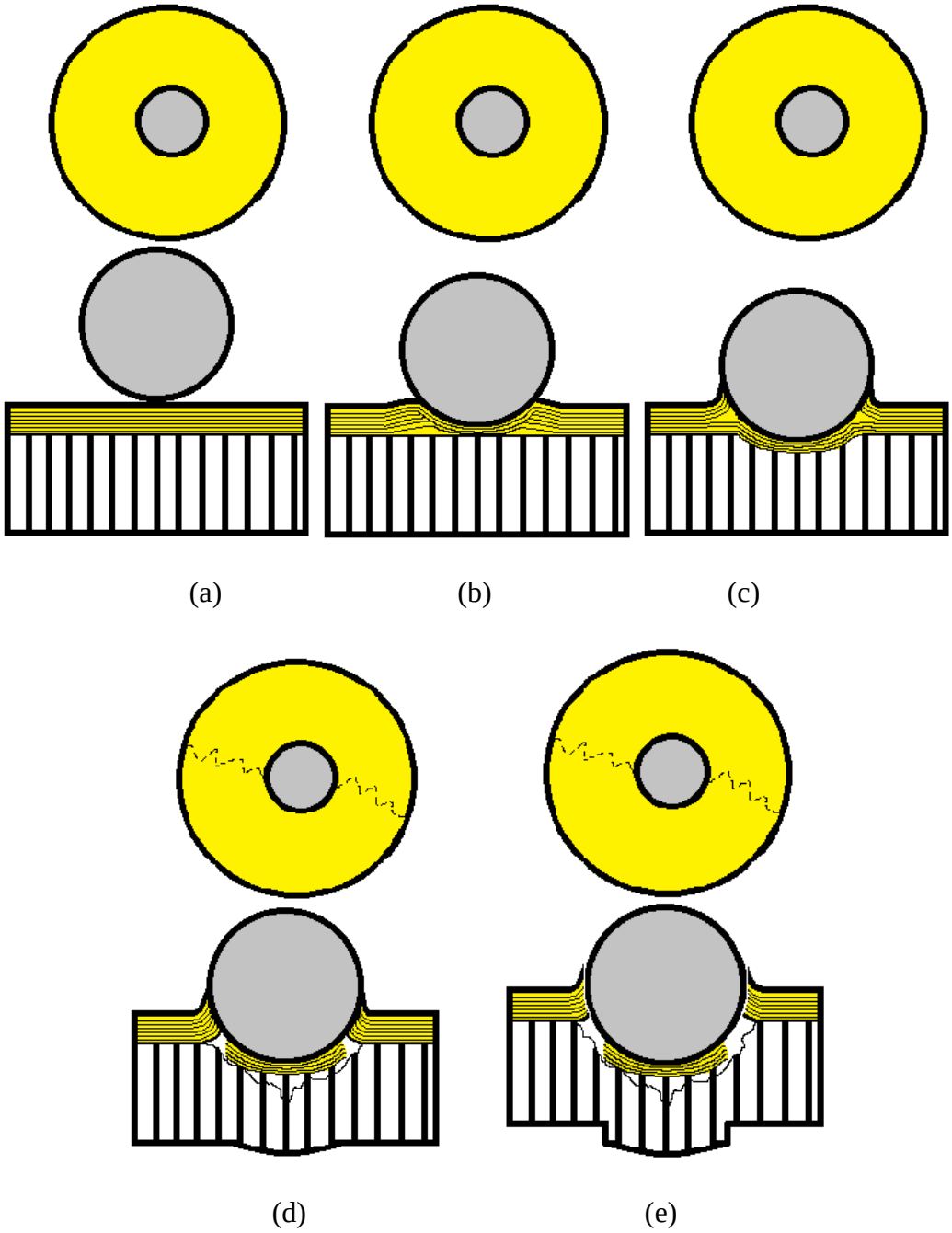

Figure 38. Top and side view of behavior of the synthetic material and bone during the small punch test

Table 11. Elastic compression moduli of bovine femur

References	Methods	Elastic modulus (GPa)	
		Longitudinal	Tangential
Reilly and Burstein [73]	Tension	23.1 (3.2)	10.4 (1.6)
	Compression	22.3 (4.6)	10.1 (1.8)
Reilly et al. [23]	Tension	21.2 (4.15)	-
	Compression	20.9 (3.26)	-
Currey [71]	Bending	18.49 (2.84)	-
Rho and Pharr [74]	Nano indentation	24.4 (2.2)	-

Table 12. Elastic compression moduli of human tibia

References	Methods	Elastic modulus (GPa)
Cowin [75]	-	17.4
Rho et al. [76, 77]	Tensile test	18.6 (3.5)
	Ultra sonic test	20.7 (1.9)
	Nano indentation	22.5 (1.3)
Z. Fan et al. [78]	Nano indentation	25.1 (2.1)

5.3.2. Displacement at maximum load and slope

The displacement of the layer-by-layer synthetic material at the maximum load was improved compared to the tumor-free human bone. The synthetic material is more deformable than tumor-free bone. This means that the synthetic material can sustain more

load. This synthetic material can protect the bone without deformation when the bone is deformed by an external force or impact. For the slope of the plots obtained via the small punch test, the slope of the synthetic material is two times higher than that of the cancerous bone. The synthetic material is stiffer than the cancerous bone. This means that the synthetic material has potential to sustain a force more than the cancerous bone at the same displacement. It is apparently promising for the synthetic material to improve the mechanical properties of bone overall.

CHAPTER VI

CONCLUSIONS AND FUTURE RECOMMENDATIONS

6.1. Conclusions

This research studied the failure mechanisms and the mechanical properties of bovine femur and human tibias and developed a synthetic material. The bovine bone samples machined in three different directions underwent the small punch test to measure the mechanical properties and to obtain fractured surfaces of the bones. Tumor-free human bone and cancerous human bone were small punch tested to investigate the effect of the cancer. The fractured surfaces of bones were observed by an optical microscope and a scanning electron microscope. Findings are summarized in the following:

1. Higher than 50%wt of concentration and longer than 5minutes of treatment time of isopropyl alcohol is an appropriate condition of the chemical solution to decontaminate bone samples.
2. The elastic moduli of bovine bone and human bone via the small punch test were in the range of 18.2~24.4 and 17.4~25.1 GPa, respectively, which were the values similar to published values.
3. Failure mechanism during small punch test in the longitudinal direction is tearing, separating and pushing out and that of radial directions is more likely breaking mechanism.
4. Cancer cells lowers density by 25% and elastic modulus by 99% in tumor-free human bone.

5. The layer-by-layer synthetic material has an 83% higher deformability than tumor-free human bone, a 136% higher deformability than bovine bone and a 99% higher stiffness than cancerous human bone.

The observation of the failure mechanism of bones in the small scale mechanical test is significant in this research. The longitudinal failure mechanism is tearing, and the tangential failure mechanism is breaking. Also, the fibrous behavior of human bone was introduced via a SEM image. The small punch test was introduced as a new feasible method to determine the mechanical properties of bones. The sample size required by the small punch test was easy to manage and small enough to repeat tests.

6.2. Limitations

First of all, because of their rarity, only two varying human bone could be tested. It was quite unfair to compare those two human bone samples because their age and gender were different; 51-year old male and 12-year old female. Also, the tumor-free bone had necrosis, thus this bone was not assumed to be healthy or normal. Another limitation in this research occurred during bacteria culturing experiment. The agar plates were swiped with the bovine bones under scrupulous care, but perfect protection from invisible microbes existing in the air was impossible.

6.3. Future work

The small punch test was introduced and applied to bovine femur and human tibia cortical bones as a new method, and optical microscope and SEM were used to observe the

failure mechanism. The future work concerns synthetic material and the observation of the structural behavior:

1. Improvements are needed for the synthetic material to have more biocompatible properties and enhanced mechanical properties.
2. Specimens will be tested at body temperature and in saline fluid to simulate a proximal in vivo environment.
3. Computed tomography images should be taken to observe the precise structural behavior of fractured bone and the structural alteration of unfractured bone.

REFERENCES

1. Kamachi Mudali U, Sridhar TM, Baldev R. Corrosion of bio implants. Sadhana 2003;28:601-37.

2. KG Investments. What is a bone fracture and how Is it treated? kidsgrowth.com/resources/articledetail.cfm?id=1504, 03/09/2011.

3. Tinetti ME. Clinical practice. Preventing falls in elderly persons. The New England Journal of Medicine 2003;348(1):42-9.

4. Sato M, Grese TA, Dodge JA, Bryant HU, Turner CH. Emerging therapies for the prevention or treatment of postmenopausal osteoporosis. Journal of Medicinal Chemical 1999;42(1):1-24.

5. Salernitano E, Migliaresi C. Composite materials for biomedical applications: a review. Journal of Applied Biomaterials & Biomechanics 2003;1:3-18.

6. ADAM Inc. Osteoporosis. ncbi.nlm.nih.gov/pubmedhealth/PMH0001400, 03/09/2011.

7. Goldman L, Ausiello D., eds. Cecil Medicine. Philadelphia, PA: Elsevier, 2007.

8. National Comprehensive Cancer Network, National comprehensive cancer network clinical practice guidelines in oncology: bone cancer. files.pbworks.com/download/BkD Ehl9B5c/pennfm/15690082/NCCN%20Bone%20Cancer%20Guidelines.pdf, 02/14/2011.

9. Lam DK, Sándor GK, Holmes HI, Carmichael RP, Clokie CM. Marble bone disease: a review of osteopetrosis and its oral health implications for dentists. Journal of the Canadian Dental Association 2007;73(9):839-43.

10. ADAM Inc. Osteomalacia. ncbi.nlm.nih.gov/pubmedhealth/PMH0001414, 03/092011.

11. Beck TJ, Ruff CB, Shaffer RA, Betsinger K, Trone DW, Brondine SK. Stress fracture in military recruits: gender differences in muscle and bone susceptibility factors. Bone 2000;27(3):437-44.

12. Sahar ND, Hong SI, Kohn DH. Micro- and nano-structural analyses of damage in bone. Micron 2005;36:617-29.

13. Ward KD, Klesges RC. A meta-analysis of the effects of cigarette smoking on bone mineral density. Calcified Tissue International 2001;68(5):259-70.

14. Kanis JA, Johansson H, Johnell O, Oden A, De Laet C, Eisman JA, Pols H, Tenenhouse A. Alcohol intake as a risk factor for fracture. Osteoporos International 2005;16(7)737-42.

15. Adachi JD. Corticosteroid-induced osteoporosis. American Journal of the Medical Sciences 1997;313(1):41-9.

16. NHN corp. Corticosteroid. terms.naver.com/item.nhn?dirId=706&docId=7464, 03/09/2011.

17. Vincent JFV, Currey JD. The mechanical properties of biological materials. Cambridge, NY: Cambridge University Press, 1980.

18. Currey JD. Bones: structure and mechanics. Princeton NJ: Princeton University Press, 2002.

19. Cowin SC. Bone Mechanics handbook. Boca Raton FL: CRC Press, 2001.

20. Ashman RB, Rho JY. Elastic modulus of trabecular bone material. Journal of Biomechanics 1988;21(3):177-81.

21. Antich PP, Anderson JA, Ashman RB, Dowdey JE, Gonzales J, Murry RC, Zerwekh JE, Pak CY. Measurement of mechanical properties of bone material in vitro by ultrasound reflection: methodology and comparison with ultrasound transmission. Journal of Bone and Mineral Research 1991;6(4):417-26.

22. Keaveny TM, Guo XE, Wachtel EF, McMahon TA, Hayes WC. Trabecular bone exhibits fully linear elastic behavior and yields at low strains. Journal of Biomechanics 1994; 27(9):1127-36.

23. Reilly DT, Burstein AH, Frankel VH. The elastic modulus for bone. Journal of Biomechanics 1974;7:271-5.

24. Ascenzi A, Bonucci E. The compressive properties of single osteons. The Anatomical Record 1968;161(3):377-91.

25. Ascenzi A, Baschieri P, Benvenuti A. The torsional properties of single selected osteons. Journal of Biomechanics 1994;27(7):875-84.

26. Ascenzi A, Bonucci E. The shearing properties of single osteons. The Anatomical Record 1971;172(3):499-510.

27. Ascenzi A, Baschieri P, Benvenuti A. The bending properties of single osteons. Journal of Biomechanics 1990;23(8):763-71.

28. Choi K, Kuhn JL, Ciarelli MJ, Goldstein SA. The elastic moduli of human subchondral, trabecular, and cortical bone tissue and the size-dependency of cortical bone modulus. Journal of Biomechanics 1990;23:1103-13.

29. Gupta HS, Zioupos P. Fracture of bone tissue: the 'hows' and the 'whys'. Medical Engineering & Physics 2008;30:1209-26.

30. Ziv V, Wagner HD, Weiner S. Microstructure-microhardness relations in parallel-fibered and lamellar bone. Bone 1996;18(5):417-28.

31. Huja SS, Katona TR, Moore BK, Roberts WE. Microhardness and anisotropy of the vital osseous interface and endosseous implant supporting bone. Journal of Orthopaedic Research 1998;16:54-60.

32. Ramakrishna S, Mayer J, Wintermantel E, Leong KW. Biomedical applications of polymer-composite materials: a review. Composites Science and Technology 2001;61(9):1189-224.

33. Park JB, Lakes RS. Biomaterials: an introduction. New York: Springer, 1992.

34. Hench LL, Joned JR. Biomaterials, artificial organs and tissue engineering. Boca Ranton FL: CRC Press, 2005.

35. Park JB. Biomaterials science and engineering. New York: Plenum Press, 1984.

36. Bizacumen Inc. Bone grafts - A US market analysis. reportlinker.com/p0164259/Bone-Grafts-A-US-Market-Analysis.html, 03/09/2011.

37. BBC Research. Advanced orthopedic technologies, implants and regenerative products. reportlinker.com/p096659/Advanced-Orthopedic-Technologies-Implants-and-Regenerative-Products.html, 03/09/2011.

38. Hollinger JO, Battistone GC. Biodegradable bone repair materials: synthetic polymers and ceramics. Clinical Orthopedics and Related Research 1986;207:290-305.

39. AZoM.com, Czernuszka J. Biomaterials under the microscope. Materials World 1996;4:452-53.

40. Staiger MP, Pietak AM, Huadmai J, Dias G. Magnesium and its alloys as orthopedic biomaterials: a review. Biomaterials 2006;27:1728-34.

41. Niinomi M. Metallic biomaterials. The Japanese Society for Artificial Organs 2008;11:105-10.

42. Ratner BD, Hoffman AS, Scheen FJ, Lemons JE. Biomaterials science: an introduction to materials in medicine. San Diego: Academic Press, 1996.
43. Bronzino JD. The biomedical engineering handbook. Boca Raton FL: CRC Press, 2000.

44. Dumitriu S. Polymeric biomaterials. New York: Marcel Dekker, 1994.

45. Holmes-Walker A. Life-enhancing plastics: plastics and other materials in medical applications. London: Imperial College Press, 2004.

46. Geetha M, Singh AK, Asokamani R, Gogia AK. Ti based biomaterials, the ultimate choice for orthopaedic implants: a review. Progress in Materials Science 2009;54:397-425.

47. Bozzi S, Etter AL, Baudin T, Robineau A, Goussain JC. Mechanical behaviour and microstructure of aluminum-steel sheets joined by FSSW. Texture, Stress, and Microstructure 2008;1-8

48. Daculsi G. Biphasic calcium phosphate concept applied to artificial bone, implant coating and injectable bone substitute. Biomaterials 1998;19(16):1473-78

49. Sopyan I, Mel M, Ramesh S, Khalid KA. Porous hydroxyapatite for artificial bone applications. Science and Technology of Advanced Materials 2007;8:116-23.

50. TenHuisen KS, Martin RI, Klimkiewicz M, Brown PW. Formation and properties of a synthetic bone composite: hydroxyapatite-collagen. Journal of Biomedical Materials Research 1995;29:803-10.

51. Dee KC, Bizios R. Mini-review: Proactive biomaterials and bone tissue engineering. Biotechnology and Bioengineering 1996;50:438-42.

52. CES Edupack. Epoxy/HS carbon fiber, UD composite, 0° lamina. 11/01/2010.

53. CES Edupack. Bone. 10/26/2010.

54. Parsons AJ, Ahmed I, Han N, Felfel R, Rudd CD. Mimicking Bone Structure and Function with Structural Composite Materials. Journal of Bionic Engineering 2010;7:S1-10.

55. H-E-B customer relations specialist. Personal Communication.

56. Ribeiro R, Ganguly P, Darensbourg D, Usta M, Ucisik AH, Liang H. Biomimetic study of a polymeric composite material for joint repair applications. Journal of Material Research 2007;22(6):1632-9.

57. DePaula CA, Truncale KG, Gertzman AA, Sunwoo MH, Dunn MG. Effects of hydrogen peroxide cleaning procedures on bone graft osteoinductivity and mechanical properties. Cell and Tissue Banking 2005;6:287-98.
58. Smith CB, Smith DA. Relations between age, mineral density and mechanical properties of human femoral compacta. Acta Orthopaedica 1976;47:496-502.

59. Wang X, Shen X, Li X, Agrawal CM. Age-related changes in the collagen network and toughness of bone. Bone 2002;31(1):1-7.

60. Wishart JM, Need AG, Horowitz M, Morris HA, Nordin BEC. Effect of age on bone density and bone turnover in men. Clinical Endocrinology 1995;42:141-46.

61. Balch WE, Schoberth S, Tanner RS, Wolfe RS. Acetobacterium, a new genus of hydrogen-oxidizing, carbon dioxide-reducing, anaerobic bacteria. International Journal of Systematic bacteriology 1977;27(4):355-61.

62. Vorlicek V, Exworthy LF, Flewitt PEJ. Evaluation of a miniaturized disc test for establishing the mechanical properties of low-alloy ferritic steels. Journal of Materials Science 1995;30(11):2936-43.

63. Snaders MW. In situ small scale mechanical characterization of materials under environmental effects. Master's degree thesis, Mechanical Engineering. College Station TX: Texas A&M University, 2010.

64. McMater-Carr Supply Company. Ball and Roller Bearings. mcmaster.com/#9292k29/=c9 gudt, 11/05/2010.

65. Hertz HR. On contact between elastic bodies. Collected Works 1882;1:156-171(German).

66. Ito S, Shima M, Jibiki T, Akita H. The relationship between AE and dissipation energy for fretting wear. Tribology International 2009;42:236-42.

67. Meunier A, Riot O, Christel P, Katz JL, Sedel L. Inhomegenities in anisotropic elastic constants of cortical bone. Ultrasonics Symposium 1989;1015-18.

68. Termine JD, Posner AS. Amorphous / crystalline interrelationships in bone mineral. Calcified Tissue Research 1966;1(1):8-23.

69. Posner AS. Crystal chemistry of bone mineral. Physiological Reviews 1969;49(4):760-92.

70. Kaste SC, Ahn H, Liu T, Krasin MJ, Hudson MM, Spunt SL. Bone mineral density deficits in pediatric patients treated for sarcoma. Pediatr Blood Cancer 2008;50:1032–8.

71. Currey JD. The effect of porosity and mineral content on the young's modulus of elasity of compact bone. Journal of Biomechanics 1988;21(2):131-9.

72. Schaffler MB, Burr DB. Stiffness of compact bone: effects of porosity and density. Journal of Biomechanics 1988;21(1):13-6.

73. Reilly DT, Burstein AH. The elastic and ultimate properties of compact bone tissue. Journal of Biomechanics 1975;8(6):397-405.

74. Rho JY, Pharr GM. Effects of drying on the mechanical properties of bovine femur measured by nanoindentation. Journal of Materials Science: Materials in Medicine 1999;10:485-8.

75. Martin RB, Burr DB, Sharkey NA. Skeletal research: an experimental approach. New York: Academic Press, 1979.

76. Rho JY, Ashman RB, Turner CH. Young's modulus of trabecular and cortical bone material: Ultrasonic and microtensile measurements. Journal of Biomechanics 1993;26(2):111-9.

77. Rho JY, Tsui TY, Pharr GM. Elastic properties of human cortical and trabecular lamellar bone measured by nanoindentation. Biomaterials 1997;18:1325-30.

78. Fan Z, Swadener JG, Jae-Young R, Roy ME, Pharr GM. Anisotropic properties of human tibial cortical bone as measured by nanoindentation. Journal of Orthopaedic Research 2002;20:806-10.

VITA

Name: Eunhwa Jang

Education:

- B.E., Architecture Engineering, Korea Military Academy, Republic of Korea, 2006
- M.S., Mechanical Engineering, Texas A&M University, 2011

Experience:

- Graduate research assistant, Liang research group, Mechanical engineering department, Texas A&M University, January, 2010~January, 2011
- Education Officer, Engineer Battalion of 7th division, Korea Military Academy, Republic of Korea Army, March, 2007 ~ October, 2008
- Platoon leader, Engineer Battalion of 7th division, Republic of Korea Army, June, 2006 ~ March, 2007

Contact methods:

- Email Address: violet0325@gmail.com, c15145@naver.com
- Address: Texas A&M University Department of Mechanical Engineering 3123 TAMU, College Station, TX, 77843-3123